representative limb skeletal muscle, and it corresponds to the tibialis anterior muscle in mice and humans. The muscle blocks were divided into pieces and frozen immediately in isopentane pre-cooled with liquid nitrogen.

Histological and immunohistochemical analysis

Serial transverse cryosections (10 μm thick) were stained with hematoxylin and eosin (H&E), and immunostained using anti-MHC antibodies. Immunohistochemistry was performed as described previously [17]. Cryosections were incubated with the following primary antibodies: mouse monoclonal antibodies against fast type MHC (NCL-MHCf; Novocastra), slow type MHC (NCL-MHCs), and developmental MHC (NCL-MHCd). The primary antibodies were detected using a Vectastain® ABC kit (Vector Laboratories) and then visualized with diaminobenzidine. Images were recorded using a microscope (Eclipse E600; Nikon) equipped with a CCD camera (HV-D28S; Hitachi), and fiber types of individual myofibers from 400 to 1200 per muscle were identified, based on serial sections immunostained with three types of MHC antibodies. Subsequently, the fiber number of each group was counted, and fiber sizes were also measured using Image-Pro Plus (Media Cybernetics). Furthermore, the differences in MHC expression between two groups (normal, dMHC (-) *vs* affected, dMHC (-); affected, dMHC (-) *vs* affected, dMHC (+)), between muscles (TC muscle *vs* diaphragm), or among ages (1, 2, 4, 6 months, and 1 year) were evaluated by Yates's chi-square test.

Myosin extraction and gel separation

Myosin was extracted on ice for 60 min from cryosections, as described previously [18,19]. MHC isoforms were separated on 8% SDS-polyacrylamide gels containing 30% glycerol, according to the methods described previously [19,20] with some modifications. Briefly, aliquots of 0.4 μg of total protein were loaded in each well of mini-gels (Bio-Rad). Electrophoresis was carried out at 60 V at 5°C for 48 h using upper buffer containing additional 10 mM 2-mercaptoethanol. The gels were stained with silver, and the image was scanned and analyzed using NIH image.

Results

MHC expression in TC muscle and diaphragm of adult CXMD$_J$

To investigate the relationship between the pathology and fiber types in dystrophic skeletal muscles of CXMD$_J$, we first examined histological features and MHC expression in TC muscles and diaphragms of normal and affected dogs at adult stages (10 months to 3 years old) (Fig. 1). In H&E-stained sections, affected muscles exhibited some dystrophic characteristics, such as necrosis, regeneration, cellular infiltration, fibrosis, fiber splitting, and fiber size variation. Especially, clusters of infiltrating cells were prominently observed in TC muscles, while endomysial fibrosis was predominant in diaphragms.

We next detected expression of fast and slow type MHCs for fiber type identification, and further examined developmental MHC, which means neonatal and/or embryonic MHC, as a marker of regenerating fibers (Fig. 1). In TC muscles and diaphragms of adult normal dogs, individual myofibers showed expression of either fast or slow type MHC. In affected TC muscles, the proportions of fast or slow MHC fibers were similar between normal and affected muscles. In addition, large numbers of developmental MHC-expressing fibers were observed in clusters, and many of these fibers co-expressed fast type MHC. In the affected diaphragms, the numbers of fast MHC fibers were much lower than in the normal counterparts, and slow type MHC was expressed in almost all fibers. Furthermore, the numbers of developmental MHC fibers were less than in affected TC muscle, and almost all of these fibers co-expressed slow type MHC, unlike TC muscle. These results indicated that the influences of dystrophin deficiency on MHC expression are significantly different between TC muscle and the diaphragm of CXMD$_J$, suggesting that the diaphragm would be more greatly influenced with regard to the composition of fiber types and muscle regeneration than TC muscle.

MHC expression and fiber size distribution

To further evaluate the size distribution of individual myofibers related to MHC expression, we measured transverse areas of all muscle fibers within one area in TC muscle or diaphragm of adult CXMD$_J$ (Fig. 2 and Table 1). We then analyzed three types of MHC-positive fibers (fast, slow, and hybrid) among populations of myofibers expressing fast and/or slow type MHC(s) together with or without developmental MHC, which were defined as regenerating or non-regenerating fibers, respectively. In non-regenerating fibers of affected TC muscle and diaphragm, the proportion of slow MHC fibers increased and these fibers showed a larger size distribution than those in the normal counterparts, indicating increased number and enlarged fiber size of slow fibers (Fig. 2B and Table 1). Interestingly, fast MHC fibers disappeared in the adult CXMD$_J$ diaphragm.

In regenerating fibers of both affected muscles, the distributions of all three populations shifted to smaller sizes than those in the normal counterparts, and a large number of hybrid fibers co-expressing fast and slow type MHCs were observed at a high rate (Fig. 2C and Table 1). In addition, fast MHC fibers were predominant in a regenerating population in TC muscle, while slow MHC fibers were predominant in the diaphragm except for hybrid fibers. These observations suggested that fast fibers could be more susceptible to dystrophic stress than slow fibers, and

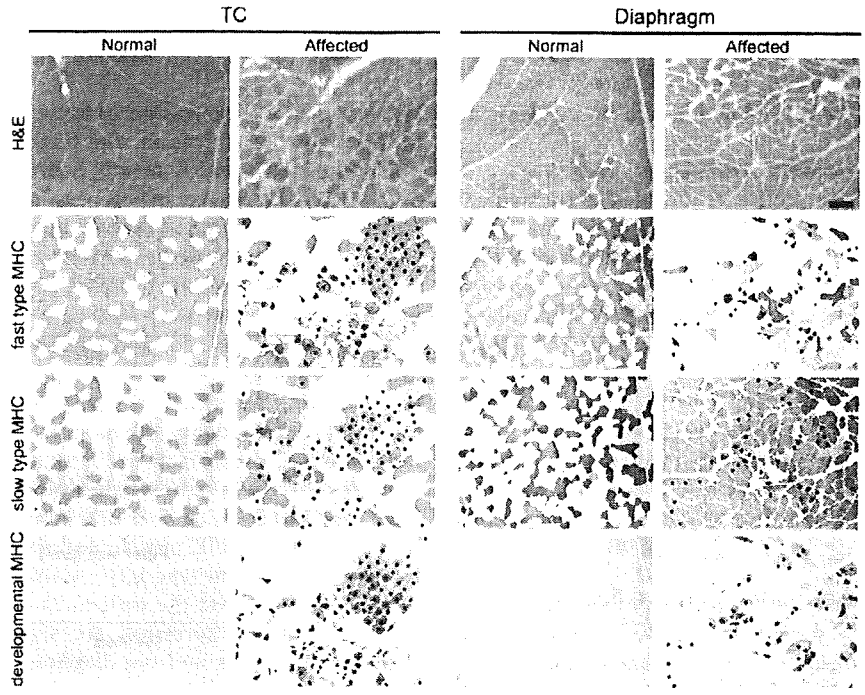

Figure 1
Representative images of histology (H&E) and expression of fast type, slow type, or developmental myosin heavy chain (MHC) in tibialis cranialis (TC) muscle and diaphragm of a normal (10 months old) or a CXMD$_J$ dog (11 months old). Identical parts of serial cross-sections are shown in longitudinal panels. In panels of affected muscles, dots show the fibers expressing developmental MHC. Bar: 200 μm.

alteration of MHC expression and regeneration of muscle fibers would be different between TC muscle and the diaphragm.

Time courses of histology and MHC expression

To investigate how MHC expression alters together with growth of CXMD$_J$, we examined MHC expression in TC muscles and diaphragms of a normal or an affected littermate at various ages from neonatal to adult stages (1 month to 1 year old) in relation to histopathological features. Affected TC muscles showed mild lesions at 1 and 2 months old, but severe degenerative lesions were evident at over 4 months old (Fig. 3). Expression of fast or slow type MHC did not alter much with aging, and developmental MHC was expressed continuously (Fig. 4). In contrast, degenerative lesions were severe in the affected diaphragm at all ages examined (from 1 month old onward), and endomysial fibrosis was dominantly present over 6 months old (Fig. 3). Fast MHC fiber number decreased markedly, while the number of slow MHC fibers increased significantly in affected diaphragms after 6 months old (Fig. 5). In addition, expression of developmental MHC decreased at 6 months and 1 year old. These observations indicated that MHC expression is altered greatly in the affected diaphragms after 6 months old, unlike TC muscles.

For quantitative evaluation of MHC expression in individual myofibers, we counted three types of MHC-expressing fibers among non-regenerating or regenerating populations within an area in the TC muscle or diaphragm of a normal or an affected littermate (Fig. 6). As normal muscles still expressed developmental MHC at 1 month old (Fig. 4 and 5), we performed the examinations at both adolescent (2 and 4 months old) and adult stages (10 or 11 months old). In normal dogs, the number of fast MHC fibers in TC muscle was three times greater than that of slow MHC fibers throughout aging, while the proportions in the diaphragms remained constant and equivalent between the two types (Fig. 6A). In non-regenerating fibers, the proportions of fiber types were not constant in affected TC muscles at the ages examined, but the majority of these fibers consisted of slow MHC fibers in the affected diaphragms (Fig. 6B). These observations indicated that slow fibers were already predominant in non-regenerating populations of CXMDJ diaphragms at younger ages. In

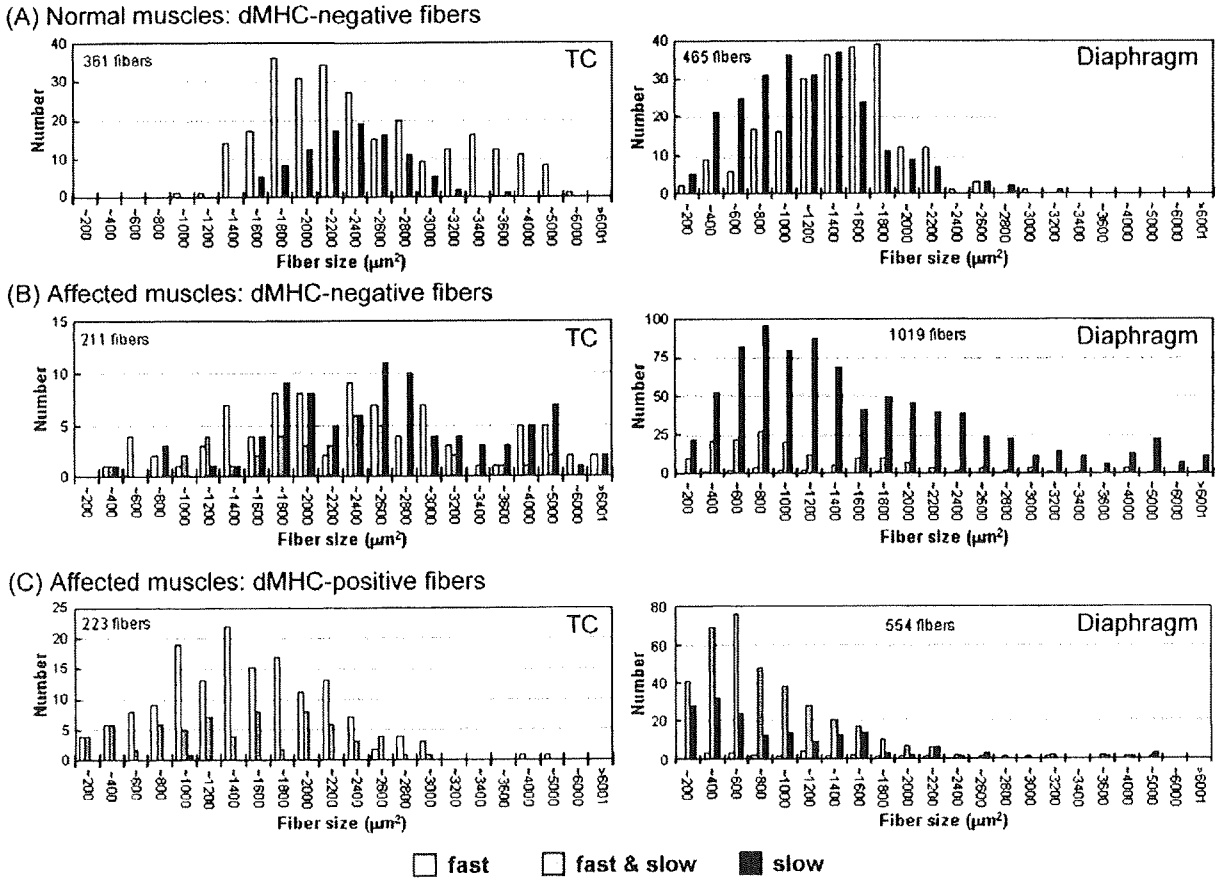

Figure 2

The size distribution of myofibers expressing fast and/or slow type MHCs in skeletal muscles of a normal (10 months old) or a CXMD$_J$ dog (11 months old). On the basis of expression of fast and slow type MHCs, all fibers within an area of TC muscle or diaphragm of a normal (A) or an affected dog (B, C) were classified into three types of MHC-positive fiber. Furthermore, fast (white), hybrid (gray), or slow MHC myofibers (black) were analyzed among populations of muscle fibers with non-expression of developmental MHC (A, B) or with expression of developmental MHC (C) in terms of fiber numbers (see Table 1) and fiber sizes (A-C). Note that larger sizes of slow MHC fibers were noticeable in populations of muscle fibers expressing fast and/or slow MHC(s) but not developmental MHC of affected muscles (B).

regenerating fibers, in contrast to the observation that fast MHC fibers consistently accounted for the majority of fibers in affected TC muscles, the affected diaphragms were mainly composed of hybrid and slow MHC fibers and the proportion increased gradually with age (Fig. 6C). These observations indicated that MHC expression in regenerating fibers was also different between affected TC muscle and diaphragm after 4 months old, although it was relatively similar in the two at 2 months old.

Temporal changes of MHC isoforms

To examine how progressive degeneration alters the composition of fiber types in affected skeletal muscles, we detected myosin isoforms in TC muscles and diaphragms of CXMD$_J$ at various ages by electrophoretic gel separation (Fig. 7). Four MHC isoforms (I, IIA, IIX, and embryonic), which migrated on electrophoresis as IIA-embryonic-IIX-I from slowest to fastest [11,12], were detected in canine skeletal muscles (Fig. 7A). In affected TC muscles, type I, IIA, and embryonic isoforms were consistently detected at similar levels, but the level of type IIX MHC was lower than those in normal TC muscles after 2 months old. In contrast, type IIA MHC level decreased gradually in affected diaphragms with growth, and type I accounted for the majority of MHC components in animals over 6 months old. In addition, the embryonic isoform

Table 1: The numbers of myofibers co-expressing fast type, slow type, and/or developmental MHCs in skeletal muscles of a normal (10 months old) or a CXMD$_J$ dog (11 months old).

	TC			Diaphragm		
	Normal	Affected		Normal	Affected	
Developmental	-	-	+	-	-	+
Fast	265 (73%)	85 (40%)	155 (70%)	222 (48%)	12 (1%)	20 (3.6%)
Fast & slow	0 (0%)	38 (18%)	67 (30%)	0 (0%)	160 (16%)	370 (66.8%)
Slow	96 (27%)	88 (42%)	1 (0%)	243 (52%)	847 (83%)	164 (29.6%)
Total	361 (100%)	211 (49%)	223 (51%)	465 (100%)	1019 (65%)	554 (35%)

The numbers of fibers analyzed were results from a normal or an affected dog. MHC expression between two groups (normal, dMHC (-) *vs* affected, dMHC (-); affected, dMHC (-) *vs* affected, dMHC (+)), or between muscles (TC muscle *vs* diaphragm) was analyzed by Yates's chi-square test. Significant differences ($p < 0.05$) were detected in all tests.

decreased in affected diaphragms after 6 months old. These results were consistent with those of immunohistochemical analyses (Figs. 4 and 5). These observations suggested that type IIX and IIA fast fibers may be preferentially affected in TC muscle and diaphragm of CXMD$_J$, respectively. Furthermore, these observations suggested that muscle regeneration may deteriorate from relatively younger age in the affected diaphragm, unlike TC muscle.

Discussion

To investigate the alterations in fiber types in skeletal muscles of a canine DMD model, we examined MHC expression in the TC muscle and diaphragm of CXMD$_J$ at various ages. Our results indicated that the influences of dys-

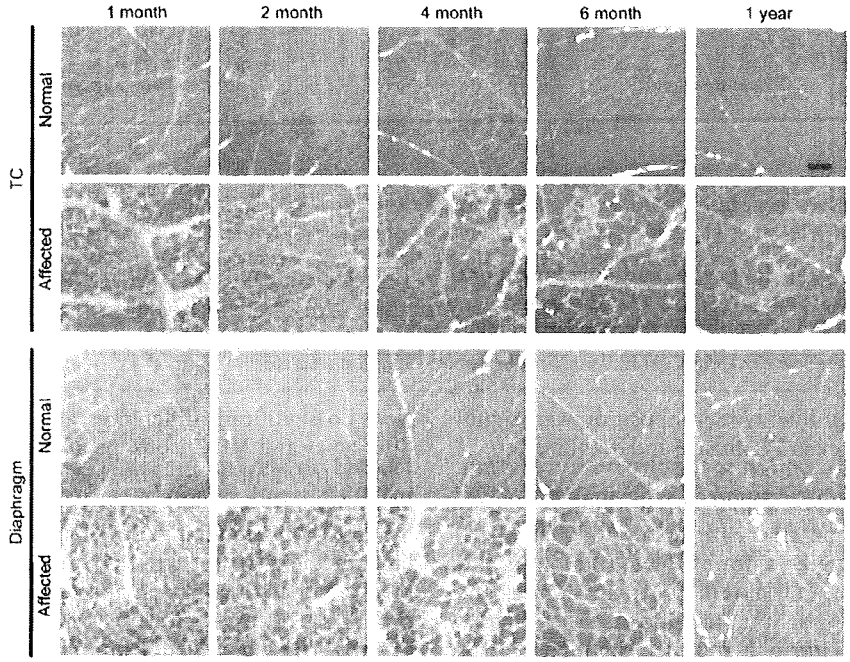

Figure 3
Representative histological findings in TC muscles and diaphragms of a normal or a CXMD$_J$ dog at 1, 2, 4, 6 months, and 1 year old. Note that severe degenerative lesions were observed from early ages in affected diaphragms, as compared with affected TC muscles. Bar: 200 μm.

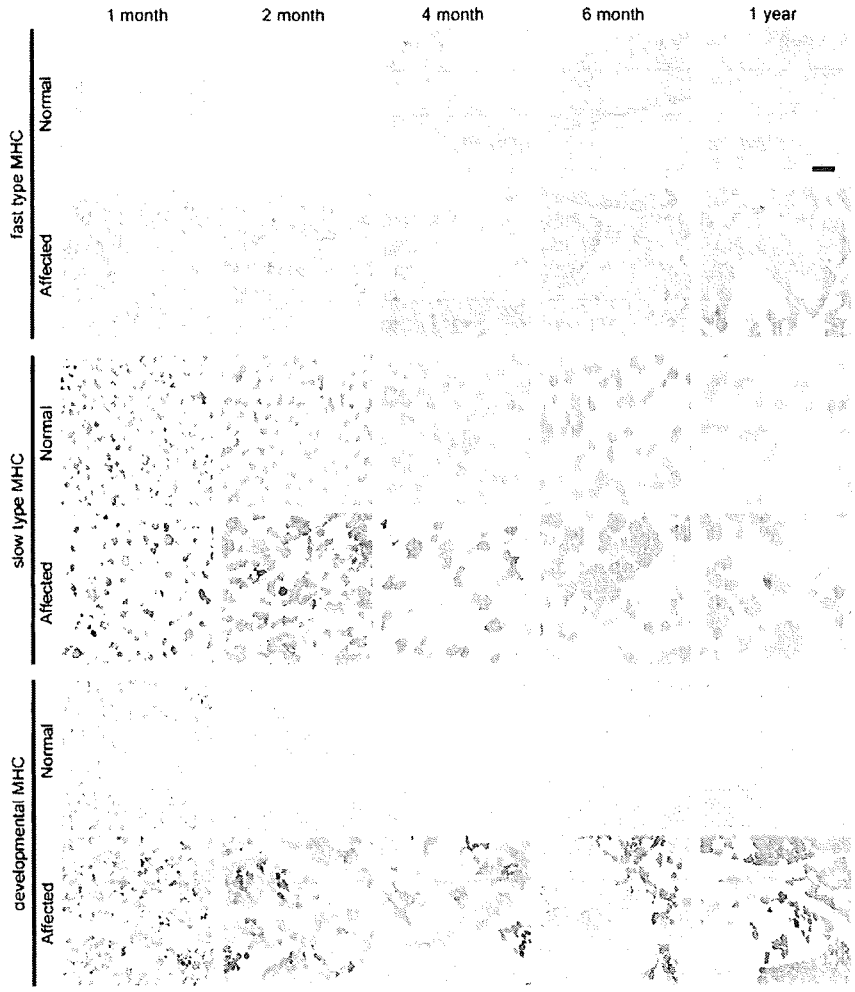

Figure 4
Expression of fast type, slow type, and developmental MHCs in TC muscles of a normal or a CXMD$_J$ dog at 1, 2, 4, 6 months, and 1 year old. Note that there were no notable differences between expression levels of fast and slow type MHCs in normal and affected TC muscles. Bar: 200 μm.

trophin deficiency on fiber type composition were significantly different between TC muscle and diaphragm.

To analyze MHC expression in details, we compared fiber type composition and fiber size distribution of MHC-expressing fibers between a normal dog (10 months old) and an affected dog (11 months old). In normal and affected dogs, body weight rapidly increased to approximately 9 kg at 4 months old, and then slightly increased to approximately 14 and 11 kg at 12 months old, respectively [5]. As body weight reflects muscle weight, muscle mass and fiber size would not extremely change in 1 month after 4 months old, especially in normal dogs. In fact, in TC muscles or diaphragms of normal dogs, there were no significant differences among compositions of fiber types and MHC isoforms after 4 months old (Fig 6 and 7). In addition, we examined normal dogs at 11, 12 and 14 months old, and affected dogs at 10, 12, 13 and 15 months old. Normal muscles of adult dogs showed similar expression of fast type, slow type, or developmental MHC at all adult ages, and affected muscles also showed similar MHC expression at examined ages (data not shown). These observations implied that there would be no significant difference in MHC expression between at 10 and 11 months old, in both of normal and affected dogs.

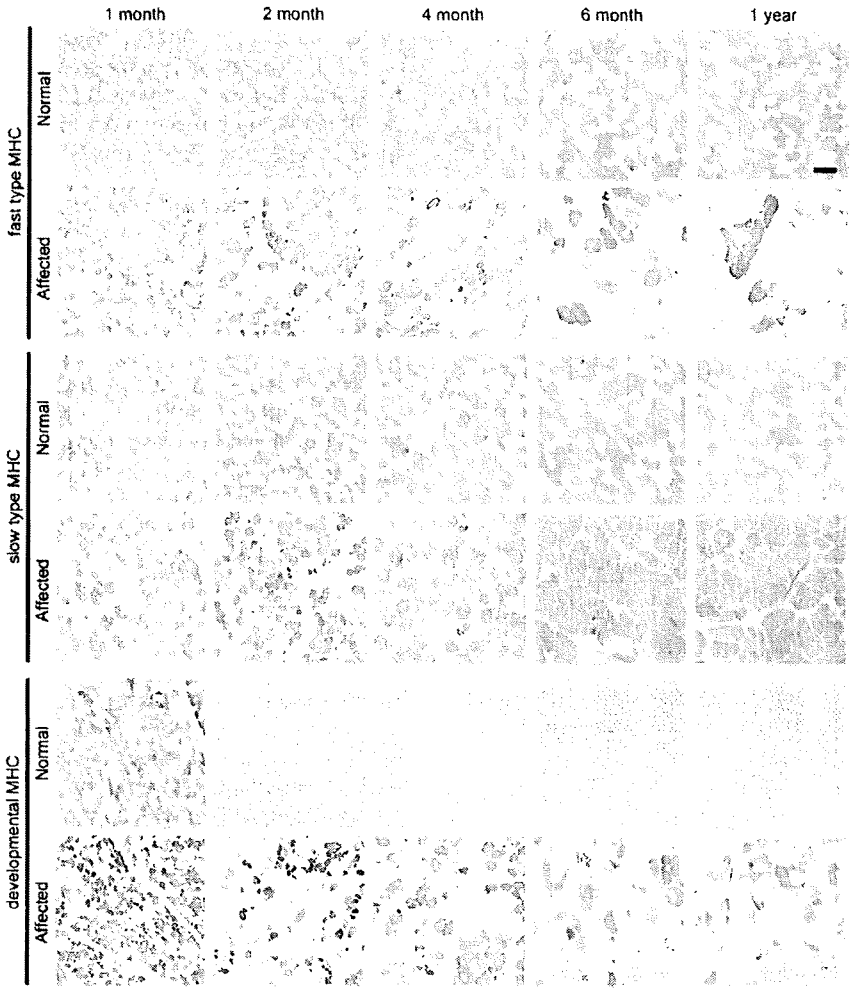

Figure 5
Expression of fast type, slow type, and developmental MHCs in diaphragms of a normal or a CXMD$_J$ dog at 1, 2, 4, 6 months, and 1 year old. Note that slow MHC fibers were increased markedly in the affected diaphragms after 6 months old, while fast MHC fibers were decreased. Bar: 200 μm.

Common features between TC muscle and diaphragm of CXMD$_J$

TC muscle and diaphragm of CXMD$_J$ shared the features that slow MHC fibers increased and enlarged selectively in non-regenerating populations, while fast type IIX or IIA MHC isoform decreased. Similar observations have been reported in skeletal muscles of the *mdx* mouse [13], GRMD [14], and human DMD [12,21]. In general, increasing and enlarging of slow fibers may be a consequence of adaptive responses by metabolic enzyme systems and energy consumption, because slow fibers have lower capacity for power output and consume less energy than fast fibers [22]. Our results also supported the hypothesis that slow fibers would be more adaptable to dystrophic stress than fast fibers, to compensate for the reduced abilities of muscle function.

Two mechanisms were considered to explain the selective increase in slow fibers during progressive muscle degeneration. One possibility is that slow fibers may be more resistant to dystrophic stress than fast fibers, leading to selective survival of slow fibers. This was supported by the observation that slower muscle fibers contained significantly more utrophin, a homolog of dystrophin, in comparison to faster counterparts [23,24]. Another is transition of MHC isoforms, where type IIA or IIX MHC

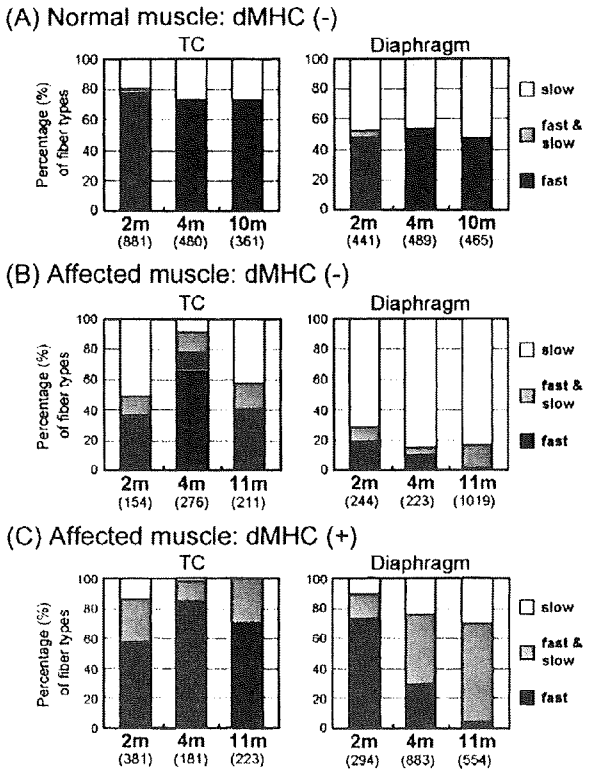

Figure 6

Proportions of fiber types in skeletal muscles of a normal or a CXMD$_J$ dog at various ages. The numbers of fast (black), hybrid (gray), and slow MHC myofibers (white) among populations of myofibers without developmental MHC (A, B) and with developmental MHC (C) were counted in TC muscle and diaphragm of a normal (A) or an affected dog (B, C) at adolescent (2 or 4 months old) or adult stages (10 or 11 months old). The numbers under the ages show total fibers examined. MHC expression between two groups (normal, dMHC (-) *vs* affected, dMHC (-); affected, dMHC (-) *vs* affected, dMHC (+)), between muscles (TC muscle *vs* diaphragm), or among ages (2, 4, and 10 or 11 months) was analyzed by Yates's chi-square test. Significant differences ($p < 0.05$) were detected in all tests, except for no significant differences between 4 and 10 months old in normal TC muscles or diaphragms. Note that slow MHC fibers were consistently larger than other fibers, in populations of muscle fibers without developmental MHC of affected diaphragms. In populations of muscle fibers co-expressing developmental MHC and other MHC isoform(s), slow MHC and hybrid fibers were increased markedly in the affected diaphragm at 4 and 11 months old, unlike TC muscles.

isoforms could be transited to type I, as seen in hypertrophy and exercise [25]. MHC I, IIa, IIx, and IIb gene expression are known to be regulated by the calcineurin pathway [26,27]. Dystrophin deficiency may accelerate MHC transition to slower types *via* calcineurin/NFAT signaling in skeletal muscles of CXMD$_J$, because calcineurin and activated NFATc1 protein content were higher in muscles from *mdx* than wild-type mice [28]. However, it remains possible that both mechanisms may be active at the same time, because the calcineurin/NFAT cascade can regulate not only the MHC promoters but also the utrophin A promoter [24,29,30].

Differences between TC muscle and diaphragm of CXMD$_J$

The CXMD$_J$ diaphragm developed severe degenerative lesions from earlier stages than TC muscle, which corresponded to previous reports [3,5,31]. In addition, dystrophic changes in the CXMD$_J$ diaphragm not only markedly altered the expression of fast and slow type MHCs but also decreased the amount of the developmental (embryonic and/or neonatal) MHC with growth, unlike affected TC muscle. Especially, fast MHC fibers disappeared and slow MHC fibers enlarged in the adult CXMD$_J$ diaphragm. The greater cross-sectional area of slow fibers in affected diaphragms might be due to hypertrophy in compensation for loss of fast fibers, relating to plasticity of muscle fibers, as mentioned above. The diaphragm keeps continuous contraction of muscle fibers without resting, while limb skeletal muscle regularly rests its movement. Therefore, replacement with slow fibers may be particularly enhanced in the diaphragm rather than TC muscle, depending on pathological severity and contractile activity of skeletal muscles.

Fiber type determination and fiber type-specific gene expression are regulated by multiple signaling pathways and transcription factors. As partially described above, a key mediator, calcineurin, plays an important role in acquisition of fiber phenotype [29,30] and may induce not only transition of MHC isoforms from faster to slower types but also transformation of myofiber phenotypes in mouse or rat muscles [26,27,32]. In addition, calcineurin signaling activity was greater in the diaphragm than in the tibialis anterior muscle of the *mdx* mouse [28]. Therefore, replacement with slow fibers may be up-regulated to a greater extent in the diaphragm than in the TC muscle of CXMD$_J$.

We also showed age-related changes of MHC expression in affected diaphragms after 6 months old, in contrast to TC muscles (Fig 4, 5 and 7). In addition, fiber type compositions in non-regenerating or regenerating fibers were also different between the TC muscle and the diaphragm, depending on age. In non-regenerating fibers of affected TC muscles, fast MHC fibers at 4 months old was higher than those at 2 and 11 months old (Fig. 6B). It might be partially involved in pathological changes that degenerative lesions appeared obviously in affected TC muscles after 4 months old, as described previously [3,5,31]. In

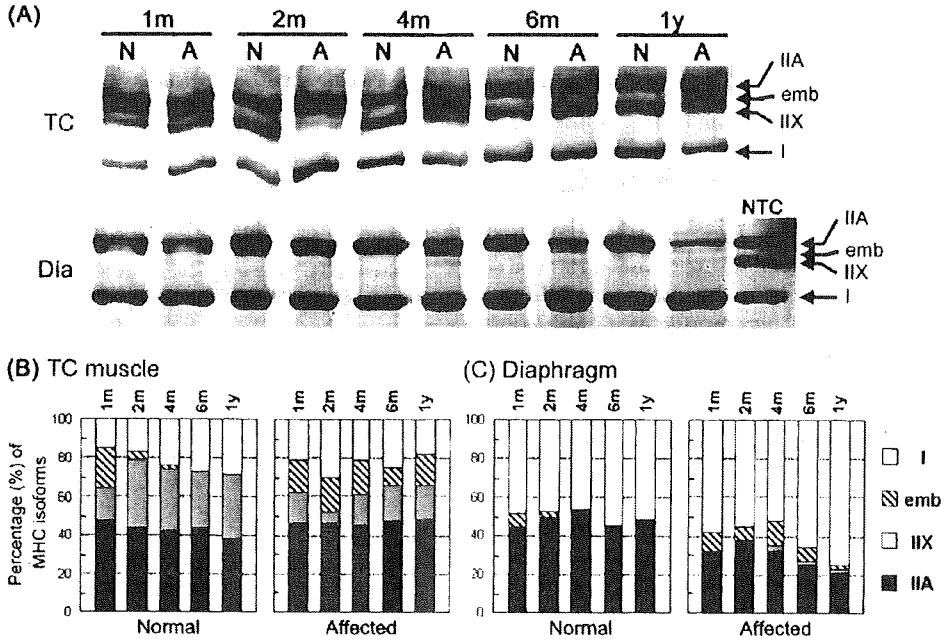

Figure 7

MHC isoforms in skeletal muscles of normal and CXMD$_J$ dogs. (A) Electrophoretic separation of MHC isoforms in TC muscle and diaphragm. Myosin was extracted from muscles at various ages (1, 2, 4, 6 months, and 1 year old), and aliquots of 0.4 μg of protein were separated on 8% SDS-polyacrylamide gels containing 30% glycerol. Four MHC isoforms (I, IIX, IIA, and embryonic) were detected. NTC: normal TC muscle at 1 year old. Note that MHC type I increased in the affected diaphragm after 6 months old. (B) Quantitative analysis of MHC isoforms. MHC expression between two groups (normal *vs* affected) or among ages (1, 2, 4, 6 months and 1 year) was analyzed by Yates's chi-square test. Significant differences ($p < 0.05$) were detected between normal and affected groups in TC muscles after 2 months old or in diaphragms after 4 months old, and between 1 and 2 months old in normal TC muscles.

regenerating fibers of the CXMD$_J$ diaphragm, the proportion of myofibers expressing slow type MHC increased markedly after 4 months old (Fig. 6C). These results suggested that MHC expression in TC muscle and the diaphragm of CXMD$_J$ would be influenced by different mechanisms after 4 months old. These age-dependent MHC expression might be related to body growth, particularly increasing of muscle mass. One possibility is participation of insulin-like growth factor (IGF)-1, which is important for postnatal growth of skeletal muscles [33] and can activate multiple Ca^{2+}-dependent signaling pathways, including the calcineurin/NFAT pathway [30]. When growth rate of body weight decreases after 4 months old [5], signaling activity of IGF-1 might reduce and MHC expression might be regulated predominantly by alternative signaling pathways.

Comparison among mdx, CXMD$_J$ and DMD diaphragms

MHC expression in normal skeletal muscle has been well studied in mice [15,34], dogs [11], and humans [35]. In normal dogs, the proportions of fiber types in TC muscle were relatively similar to those in the representative tibialis anterior muscles of mice and humans. In the diaphragm, however, the proportion of fiber types differed markedly among these species. The murine diaphragm is composed mainly of fast type IIA and IIX isoforms [15,34], but the canine diaphragm consists of equal populations of slow type MHC I and fast type MHC IIA [11], as also shown in our study. In normal human diaphragm, the distribution of myosin isoforms has been estimated that types I, IIA, and IIX account for approximately 45%, 40%, and 15%, respectively [35]. Thus, the proportions of MHC isoforms in the diaphragm of healthy dogs are much closer to those of humans than those of mice.

Some groups have studied expression profiles of MHC isoforms in the diaphragm of the *mdx* mouse. The *mdx* diaphragm shows increases in MHC type I fibers and elimination of type IIX population at 2 years old, but not at young ages (3 to 6 months old) [13,15,34]. In contrast to the *mdx* diaphragm, that in CXMD$_J$ exhibited drastic changes even in younger animals (6 months old). On the

other hand, there is no direct information available regarding the changes in fiber type composition in the diaphragm in human DMD. In addition, there is an important difference of MHC expression even in limb skeletal muscles between large mammals (including dogs and humans) and mammals with smaller body mass, especially rodents. The former do not express the fastest MHC IIB isoform in limb muscles [10,11,36], while it is abundantly expressed in the latter [34]. Therefore, changes/adaptations in skeletal muscles of dogs with muscular dystrophy are likely to be more relevant to human DMD, than that in the *mdx* mouse. As it is difficult to examine the diaphragms of DMD patients, it would be important to investigate the differences between murine and canine models for understanding the mechanisms of respiratory failure in human DMD.

Conclusion

Based on fiber type classification using MHC expression, we demonstrated the predominant replacement with slow fibers and reduced muscle regeneration with progression of muscular dystrophy in the diaphragm of a canine DMD model, but these phenomena were much less strict in affected TC muscle. In addition, the expression profiles of MHC isoforms in the $CXMD_J$ diaphragm were evidently different from those of the *mdx* mouse. Our results indicated that dystrophic dog is a more appropriate model than a murine one for human DMD, and would be useful for investigation of the mechanisms of respiratory failure in DMD, as well as pathological and molecular biological backgrounds, and therapeutic effects in clinical trials.

Competing interests

The author(s) declare that they have no competing interests.

Authors' contributions

KY designed the study, carried out the pathological and immunohistological examinations, and drafted the manuscript. AN participated in interpretation of data, and helped to draft the manuscript. TH participated in coordination of the study. ST participated in the design, planning, and coordination of the study, and helped to draft the manuscript. All authors read and approved the final manuscript.

Acknowledgements

We are grateful to Dr. Madoka Yoshimura, Dr. Nobuyuki Urasawa, Dr. Naoko Yugeta, Ms. Ryoko Nakagawa, and Dr. Masayuki Tomohiro for technical assistance. We also thank Mr. Hideki Kita and Mr. Shinichi Ichikawa for care and management of experimental animals. This work was supported by Grants-in-Aid for Center of Excellence (COE), Research on Nervous and Mental Disorders (13B-1, 16B-2, 17A-10, 19A-7), Health Science Research Grants for Research on Psychiatry and Neurological Disease and Mental Health (H12-kokoro-025, H15-kokoro-021, H18-kokoro-019), and the Human Genome and Gene Therapy (H13-genome-001, H16-genome-003) from the Ministry of Health, Labor, and Welfare of Japan, and Grants-in-Aid for Scientific Research to KY and High-Tech Research Center Project for Private Universities (matching fund subsidy, 2004-2008) from the Ministry of Education, Culture, Sports, Science, and Technology of Japan.

References

1. Emery AEH: *Duchenne Muscular Dystrophy* 2nd edition. Oxford: Oxford University Press; 1993.
2. Nonaka I: **Animal models of muscular dystrophies.** *Lab Anim Sci* 1998, **48**:8-17.
3. Valentine BA, Cooper BJ, Cummings JF, De Lahunta A: **Canine X-linked muscular dystrophy: morphologic lesions.** *J Neurol Sci* 1990, **97**:1-23.
4. Howell JM, Fletcher S, Kakulas BA, O'Hara M, Lochmuller H, Karpati G: **Use of the dog model for Duchenne muscular dystrophy in gene therapy trials.** *Neuromuscul Disord* 1997, **7**:325-328.
5. Shimatsu Y, Yoshimura M, Yuasa K, Urasawa N, Tomohiro M, Nakura M, Tanigawa M, Nakamura A, Takeda S: **Major clinical and histopathological characteristics of canine X-linked muscular dystrophy in Japan, CXMDJ.** *Acta Myol* 2005, **24**:145-154.
6. Shimatsu Y, Katagiri K, Furuta T, Nakura M, Tanioka Y, Yuasa K, Tomohiro M, Kornegay JN, Nonaka I, Takeda S: **Canine X-linked muscular dystrophy in Japan (CXMDJ).** *Exp Anim* 2003, **52**:93-97.
7. Yugeta N, Urasawa N, Fujii Y, Yoshimura M, Yuasa K, Wada MR, Nakura M, Shimatsu Y, Tomohiro M, Takahashi A, Machida N, Wakao Y, Nakamura A, Takeda S: **Cardiac involvement in Beagle-based canine X-linked muscular dystrophy in Japan (CXMDJ): electrocardiographic, echocardiographic, and morphologic studies.** *BMC Cardiovasc Disord* 2006, **6**:47.
8. Fukushima K, Nakamura A, Ueda H, Yuasa K, Yoshida K, Takeda S, Ikeda S: **Activation and localization of matrix metalloproteinase-2 and -9 in the skeletal muscle of the muscular dystrophy dog (CXMDJ).** *BMC Musculoskelet Disord* 2007, **8**:54.
9. Yuasa K, Yoshimura M, Urasawa N, Ohshima S, Howell JM, Nakamura A, Hijikata T, Miyagoe-Suzuki Y, Takeda S: **Injection of a recombinant AAV serotype 2 into canine skeletal muscles evokes strong immune responses against transgene products.** *Gene Ther* 2007, **14**:1249-1260.
10. Scott W, Stevens J, Binder-Macleod SA: **Human skeletal muscle fiber type classifications.** *Phys Ther* 2001, **81**:1810-1816.
11. Toniolo L, Maccatrozzo L, Patruno M, Pavan E, Caliaro F, Rossi R, Rinaldi C, Canepari M, Reggiani C, Mascarello F: **Fiber types in canine muscles: myosin isoform expression and functional characterization.** *Am J Physiol Cell Physiol* 2007, **292**:C1915-1926.
12. Marini JF, Pons F, Leger J, Loffreda N, Anoal M, Chevallay M, Fardeau M, Leger JJ: **Expression of myosin heavy chain isoforms in Duchenne muscular dystrophy patients and carriers.** *Neuromuscul Disord* 1991, **1**:397-409.
13. Muller J, Vayssiere N, Royuela M, Leger ME, Muller A, Bacou F, Pons F, Hugon G, Mornet D: **Comparative evolution of muscular dystrophy in diaphragm, gastrocnemius and masseter muscles from old male *mdx* mice.** *J Muscle Res Cell Motil* 2001, **22**:133-139.
14. Lanfossi M, Cozzi F, Bugini D, Colombo S, Scarpa P, Morandi L, Galbiati S, Cornelio F, Pozza O, Mora M: **Development of muscle pathology in canine X-linked muscular dystrophy. I. Delayed postnatal maturation of affected and normal muscle as revealed by myosin isoform analysis and utrophin expression.** *Acta Neuropathol* 1999, **97**:127-138.
15. Petrof BJ, Stedman HH, Shrager JB, Eby J, Sweeney HL, Kelly AM: **Adaptations in myosin heavy chain expression and contractile function in dystrophic mouse diaphragm.** *Am J Physiol* 1993, **265**:C834-841.
16. Honeyman K, Carville KS, Howell JM, Fletcher S, Wilton SD: **Development of a snapback method of single-strand conformation polymorphism analysis for genotyping Golden Retrievers for the X-linked muscular dystrophy allele.** *Am J Vet Res* 1999, **60**:734-737.
17. Yuasa K, Sakamoto M, Miyagoe-Suzuki Y, Tanouchi A, Yamamoto H, Li J, Chamberlain JS, Xiao X, Takeda S: **Adeno-associated virus vector-mediated gene transfer into dystrophin-deficient skeletal muscles evokes enhanced immune response against the transgene product.** *Gene Ther* 2002, **9**:1576-1588.

18. Butler-Browne GS, Whalen RG: **Myosin isozyme transitions occurring during the postnatal development of the rat soleus muscle.** *Dev Biol* 1984, **102**:324-334.
19. Hosaka Y, Yokota T, Miyagoe-Suzuki Y, Yuasa K, Imamura M, Matsuda R, Ikemoto T, Kameya S, Takeda S: **Alpha1-syntrophin-deficient skeletal muscle exhibits hypertrophy and aberrant formation of neuromuscular junctions during regeneration.** *J Cell Biol* 2002, **158**:1097-1107.
20. Agbulut O, Li Z, Mouly V, Butler-Browne GS: **Analysis of skeletal and cardiac muscle from desmin knock-out and normal mice by high resolution separation of myosin heavy-chain isoforms.** *Biol Cell* 1996, **88**:131-135.
21. Webster C, Silberstein L, Hays AP, Blau HM: **Fast muscle fibers are preferentially affected in Duchenne muscular dystrophy.** *Cell* 1988, **52**:503-513.
22. Crow MT, Kushmerick MJ: **Chemical energetics of slow- and fast-twitch muscles of the mouse.** *J Gen Physiol* 1982, **79**:147-166.
23. Gramolini AO, Belanger G, Thompson JM, Chakkalakal JV, Jasmin BJ: **Increased expression of utrophin in a slow vs. a fast muscle involves posttranscriptional events.** *Am J Physiol Cell Physiol* 2001, **281**:C1300-1309.
24. Chakkalakal JV, Stocksley MA, Harrison MA, Angus LM, Deschenes-Furry J, St-Pierre S, Megeney LA, Chin ER, Michel RN, Jasmin BJ: **Expression of utrophin A mRNA correlates with the oxidative capacity of skeletal muscle fiber types and is regulated by calcineurin/NFAT signaling.** *Proc Natl Acad Sci USA* 2003, **100**:7791-7796.
25. Gregory P, Low RB, Stirewalt WS: **Changes in skeletal-muscle myosin isoenzymes with hypertrophy and exercise.** *Biochem J* 1986, **238**:55-63.
26. Dunn SE, Burns JL, Michel RN: **Calcineurin is required for skeletal muscle hypertrophy.** *J Biol Chem* 1999, **274**:21908-21912.
27. Allen DL, Sartorius CA, Sycuro LK, Leinwand LA: **Different pathways regulate expression of the skeletal myosin heavy chain genes.** *J Biol Chem* 2001, **276**:43524-43533.
28. Stupka N, Michell BJ, Kemp BE, Lynch GS: **Differential calcineurin signalling activity and regeneration efficacy in diaphragm and limb muscles of dystrophic *mdx* mice.** *Neuromuscul Disord* 2006, **16**:337-346.
29. Spangenburg EE, Booth FW: **Molecular regulation of individual skeletal muscle fiber types.** *Acta Physiol Scand* 2003, **178**:413-424.
30. Michel RN, Dunn SE, Chin ER: **Calcineurin and skeletal muscle growth.** *Proc Nutr Soc* 2004, **63**:341-349.
31. Valentine BA, Cooper BJ: **Canine X-linked muscular dystrophy: selective involvement of muscles in neonatal dogs.** *Neuromuscul Disord* 1991, **1**:31-38.
32. Chin ER, Olson EN, Richardson JA, Yang Q, Humphries C, Shelton JM, Wu H, Zhu W, Bassel-Duby R, Williams RS: **A calcineurin-dependent transcriptional pathway controls skeletal muscle fiber type.** *Genes Dev* 1998, **12**:2499-509.
33. Lupu F, Terwilliger JD, Lee K, Segre GV, Efstratiadis A: **Roles of growth hormone and insulin-like growth factor 1 in mouse postnatal growth.** *Dev Biol* 2001, **229**:141-162.
34. Coirault C, Lambert F, Marchand-Adam S, Attal P, Chemla D, Lecarpentier Y: **Myosin molecular motor dysfunction in dystrophic mouse diaphragm.** *Am J Physiol* 1999, **277**:C1170-1176.
35. Polla B, D'Antona G, Bottinelli R, Reggiani C: **Respiratory muscle fibres: specialisation and plasticity.** *Thorax* 2004, **59**:808-817.
36. Snow DH, Billeter R, Mascarello F, Carpene E, Rowlerson A, Jenny E: **No classical type IIB fibres in dog skeletal muscle.** *Histochemistry* 1982, **75**:53-65.

Pre-publication history

The pre-publication history for this paper can be accessed here:

http://www.biomedcentral.com/1471-2474/9/1/prepub

NO production results in suspension-induced muscle atrophy through dislocation of neuronal NOS

Naoki Suzuki,[1,2] Norio Motohashi,[1] Akiyoshi Uezumi,[1] So-ichiro Fukada,[1] Tetsuhiko Yoshimura,[3] Yasuto Itoyama,[2] Masashi Aoki,[2] Yuko Miyagoe-Suzuki,[1] and Shin'ichi Takeda[1]

[1]Department of Molecular Therapy, National Institute of Neuroscience, National Center of Neurology and Psychiatry, Kodaira, Tokyo, Japan.
[2]Department of Neurology, Tohoku University School of Medicine, Seiryo-machi, Sendai, Japan.
[3]Project of Biofunctional Reactive Species, Yamagata Promotional Organization of Industrial Technology, Matsuei, Yamagata, Japan.

Forkhead box O (Foxo) transcription factors induce muscle atrophy by upregulating the muscle-specific E3 ubiquitin ligases MuRF-1 and atrogin-1/MAFbx, but other than Akt, the upstream regulators of Foxos during muscle atrophy are largely unknown. To examine the involvement of the dystrophin glycoprotein complex (DGC) in regulation of Foxo activities and muscle atrophy, we analyzed the expression of DGC members during tail suspension, a model of unloading-induced muscle atrophy. Among several DGC members, only neuronal NOS (nNOS) quickly dislocated from the sarcolemma to the cytoplasm during tail suspension. Electron paramagnetic resonance spectrometry revealed production of NO in atrophying muscle. nNOS-null mice showed much milder muscle atrophy after tail suspension than did wild-type mice. Importantly, nuclear accumulation of dephosphorylated Foxo3a was not evident in nNOS-null muscle, and neither MuRF-1 nor atrogin-1/MAFbx were upregulated during tail suspension. Furthermore, an nNOS-specific inhibitor, 7-nitroindazole, significantly prevented suspension-induced muscle atrophy. The NF-κB pathway was activated in both wild-type and nNOS-null muscle during tail suspension. We also show that nNOS was involved in the mechanism of denervation-induced atrophy. We conclude that nNOS/NO mediates muscle atrophy via regulation of Foxo transcription factors and is a new therapeutic target for disuse-induced muscle atrophy.

Introduction

Reduced muscle activity such as bed rest, limb immobilization, denervation, or unloading (e.g., tail suspension or space flight) leads to significant muscle atrophy (1, 2). In these conditions, the atrophying muscles show increased rates of protein degradation mainly through activation of the ubiquitin proteasome system (3, 4), and the muscle-specific E3 ubiquitin ligases muscle-specific RING finger protein 1 (MuRF-1) and atrogin-1/muscle atrophy F-box protein (atrogin-1/MAFbx) are commonly upregulated (3, 4). Recent studies further showed that muscle inactivity results in suppression of the IGF-1/PI3K/Akt pathway (5–8) and activation of transcription factors such as the forkhead box O (Foxo) family and NF-κB (9–11).

Foxo family of forkhead transcription factors regulates a variety of biological process such as metabolism, cell proliferation and death, tumor growth, response to stress, and longevity (12–15). Mammals have 4 members, Foxo1a, Foxo3a, Foxo4, and Foxo6 (12). Among them, Foxo1a is activated in almost all forms of muscle atrophy (16). Importantly, several experiments indicate that forced expression of Foxo1a or Foxo3a upregulates the expression of a variety of atrophy-related genes including MuRF-1 and atrogin-1/MAFbx genes and induces muscle atrophy both in vitro and in vivo (4, 10, 16, 17). These observations indicate that Foxo1a and Foxo3a are central players in atrophy signaling.

The activities of Foxo factors are thought to be regulated mainly at posttranslational levels by a serine/threonine kinase Akt. In the absence of muscle activities, Akt is inactivated, leading to dephosphorylation of Foxo transcription factors. As a result, dephosphorylated Foxos enter into the nucleus and activate atrophy-inducing genes (10, 18). Conversely, when Akt is activated, Foxos are phosphorylated and bound by 14-3-3 proteins and move from nucleus to cytoplasm (13, 19).

NF-κB is another key signaling molecule in muscle atrophy. In particular, crucial roles for NF-κB in both cachexia- and inactivity-induced muscle atrophy have been well investigated (9, 20, 21).

Several molecules are proposed as a mechanical sensor or a trigger of disuse atrophy. Recently it has been reported that muscles from tumor-bearing mice exhibited reduced levels of dystrophin, the protein that is mutated in Duchenne muscular dystrophy, together with reduced levels of dystrophin-associated glycoprotein (22, 23). Furthermore, forced expression of dystrophin in transgenic mice counteracted cachexia-induced muscle atrophy (22). The role of the dystrophin glycoprotein complex (DGC) in inactivity-induced muscle atrophy is not known yet, but these results raise the possibility that the DGC works as a regulator of muscle atrophy or serves as a scaffold for anti-atrophic signal transduction.

To clarify the roles for the DGC in muscle atrophy, we examined the expression and function of the members of DGC in skeletal muscle during tail suspension, a model of unloading. Here we demonstrate that neuronal NOS (nNOS), a peripheral member of the DGC, is activated in unloading conditions, regulates Foxo3a, and promotes muscle atrophy. We also show that a nNOS-specific

Nonstandard abbreviations used: DGC, dystrophin glycoprotein complex; EPR, electron paramagnetic resonance; Foxo, forkhead box O; IKKβ, inhibitor of NF-κB kinase β; L-NAME, N-nitro-L-arginine methylester; MAFbx, muscle atrophy F-box protein; MGD, *N*-methyl-D-glucamine-dithiocarbamate; mTOR, mammalian target of rapamycin; MuRF-1, muscle-specific RING finger protein 1; 7NI, 7-nitroindazole; nNOS, neuronal NOS.

Conflict of interest: The authors have declared that no conflict of interest exists.

Citation for this article: *J. Clin. Invest.* 117:2468–2476 (2007). doi:10.1172/JCI30654.

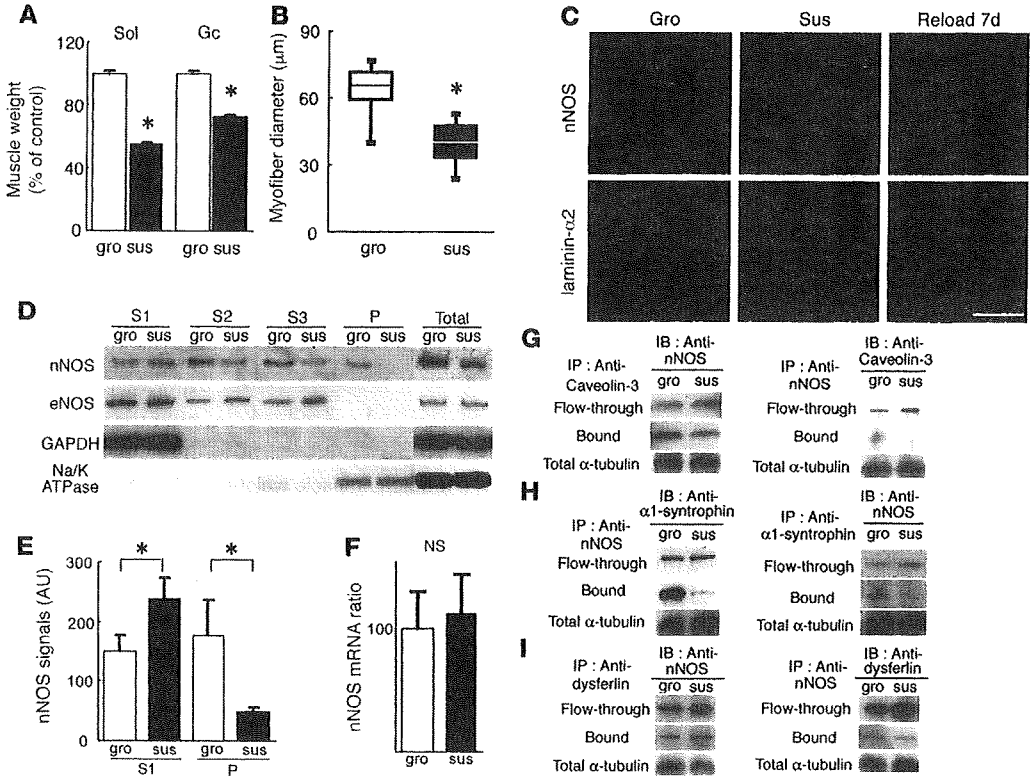

Figure 1

nNOS disappears from the sarcolemma during tail suspension. (**A**) Weights of soleus (Sol) and gastrocnemius (Gc) muscles from tail-suspended (sus) wild-type mice are normalized to body weight and are expressed as percentage of ground control (gro) (n = 15/group). *P < 0.05, Student's t test. (**B**) Box and whiskers plot of myofiber diameter size of soleus. Boxes represent the middle 50% of the data, lines represent the median, and whiskers represent the range. More than 200 fibers were measured on laminin-α2 chain–stained cross sections. (**C**) Immunofluorescent staining for nNOS and laminin-α2 chain. Transverse muscle sections from ground control mice, tail-suspended mice, and mice after reloading for 7 days (reload 7d) were stained with anti-nNOS (green) and anti–laminin-α2 chain antibodies (red). Scale bar: 50 μm. (**D**) Western blot using anti-nNOS antibody on subcellular fractions of muscle extracts. P indicates insoluble pellet after sequential extraction of skeletal muscle homogenates with 100 mM NaCl (S1), 500 mM NaCl (S2), and 0.5% Triton X-100 (S3). GAPDH signals in S1 and Na/K-ATPase signals in P confirmed that our fractionation was correctly done. Fractionation and western blotting were repeated 5 times, and representative data are presented. Note the slight increase of nNOS levels in S1 fraction and loss of nNOS signal in insoluble P fraction during tail suspension. (**E**) Quantification of nNOS signals in S1 and P fractions of muscle extracts shown in D (n = 5 /group). The signals in S1 and P fractions were normalized to GAPDH or Na/K-ATPase, respectively. Mann-Whitney, *P < 0.05. (**F**) Levels of nNOS mRNA in muscles from ground control mice and tail-suspended mice for 2 weeks were evaluated by real-time PCR (n = 5/group). No significant difference was found by Mann-Whitney test. (**G**) Immunoprecipitation with caveolin-3 antibody and immunoblot with nNOS antibody, and vice versa, for ground control and tail suspension groups. (**H**) Immunoprecipitation with α1-syntrophin Ab and immunoblot with nNOS antibody, and vice versa. (**I**) Immunoprecipitation of dysferlin antibody and immunoblot with nNOS Ab, and vice versa. In **G**–**I**, flow-through fraction was also examined by western blotting with anti–α-tubulin antibody.

inhibitor, 7-nitroindazole (7NI), significantly attenuates suspension-induced muscle atrophy. Furthermore, we show the involvement of nNOS in denervation-induced muscle atrophy process. Thus nNOS and NO are to our knowledge new therapeutic targets for disuse-induced muscle atrophy.

Results

nNOS disappears from the sarcolemma during tail suspension. To elucidate molecular mechanisms of unloading-induced muscle atrophy, we performed tail suspension (14 days) and reloading (7 days) experiments using wild-type C57BL/6 mice. The weights of the soleus and gastrocnemius (Figure 1A) muscles were decreased to 50%–70% of those of the control mice after tail suspension. The mice showed weakened grasping power and less endurance in running on the rotarod test after tail suspension (Supplemental Figure 1; supplemental material available online with this article; doi:10.1172/JCI30654DS1). The diameter of myofiber was also drastically decreased (Figure 1B). The expression patterns of the components of DGC, dystrophin, β-dystroglycan, α-sarcoglycan, dystrobrevin, laminin-α2, α1-syntrophin, and caveolin-3 were not changed during tail suspension (data not shown). The serum creatine kinase level was not elevated, and Evans blue dye uptake by myofibers was not evident in atrophied muscles (Supplemental Figure 2), indicating that the sarcolemmal integrity was maintained during tail suspension. nNOS mRNA levels were not significantly reduced (Figure 1F), and total nNOS protein was slightly decreased during tail suspension (Figure 1D). Importantly, immunohistochemistry revealed that nNOS was lost from the sarcolemma during tail suspension (Figure 1C). The sarcolemmal expression was gradually restored during the reloading process

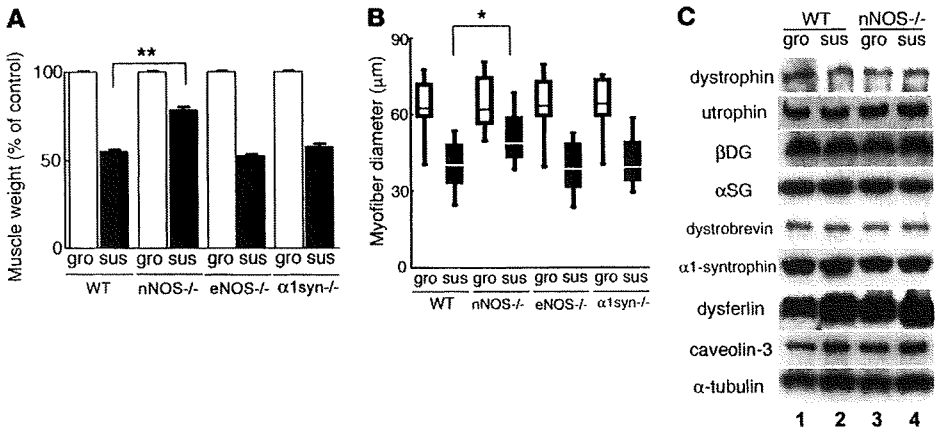

Figure 2

nNOS-null mice show partial tolerance to disuse-induced muscle atrophy. **(A)** Soleus muscle weight from ground control and tail-suspended wild-type ($n = 20$), nNOS-null ($n = 20$), eNOS-null ($n = 10$), and α1-syntrophin–null ($n = 10$) mice after 2-week tail suspension is shown as percent of wild-type ground controls. $^{**}P < 0.01$, Student's t test. **(B)** Box and whiskers plot of diameter of myofiber in soleus. Diameters were measured on H&E-stained cross sections of soleus muscles. $n = 200$ fibers in each experiment. $^{*}P < 0.05$, Student's t test. **(C)** Immunoblots of mouse gastrocnemius muscle extracts for DGC components from wild-type ground control (lane 1), wild-type tail-suspended (lane 2), nNOS-null ground control (lane 3), and nNOS-null tail-suspended (lane 4) mice. All lanes contain 30 μg of total protein. The experiments were performed 5 times, and representative pictures are presented.

(Figure 1C). eNOS expression was not changed (Figure 1D), and iNOS was not expressed (data not shown) during the course.

Next we performed subcellular fractionation of muscle homogenates as described previously (24). In ground control mice, nNOS remained in the insoluble pellet (Figure 1D). In tail-suspended mice, nNOS was largely extracted with 100 mM NaCl and barely detected in the pellet fraction (Figure 1D). Quantification of nNOS bands clearly showed that nNOS dislocated from the sarcolemma to the cytoplasm during tail suspension (Figure 1E). These results indicate that nNOS exists mainly in the cytoplasm during tail suspension. Immunoprecipitation experiments also revealed that nNOS completely dissociated from α1-syntrophin and caveolin-3 during tail suspension (Figure 1, G and H). In contrast, a considerable amount of dysferlin was immunoprecipitated with nNOS antibody during tail suspension (Figure 1I).

nNOS-null mice represent tolerance to disuse-induced muscle atrophy. To examine the roles of dislocated nNOS in muscle atrophy, we then performed tail suspension experiments using wild-type, nNOS-null, eNOS-null, and α1-syntrophin–null mice. The body weight (Figure 2A), average muscle fiber diameter (Figure 2B), and total number of muscle fibers (data not shown) of nNOS-null mice in the ground condition were similar to those of wild-type mice. However, after tail suspension for 14 days, reduction of muscle weight (Figure 2A), muscle size (Figure 2B), and muscle power (Supplemental Figure 1) were significantly less severe in the nNOS-null mice. Except for nNOS, dystrophin and other components of DGC were expressed in nNOS-null muscle at the same level as in wild-type muscle in both ground and suspended conditions (Figure 2C). eNOS-null muscle revealed atrophy during tail suspension similar to that seen in wild-type muscle (Figure 2, A and B), indicating that eNOS is not essential for atrophy signaling. We previously reported that disruption of the α1-syntrophin gene resulted in dislocation of nNOS from the sarcolemma to the cytoplasm without dystrophic phenotypes (25, 26). Suspension of α1-syntrophin–null mice induced severe muscle atrophy as it did in wild-type muscle (Figure 2, A and B).

Production of NO by nNOS in tail-suspended skeletal muscle. To directly measure the levels of NO in skeletal muscle during tail suspension, we employed electron paramagnetic resonance (EPR) spectrometry with *N*-methyl-D-glucamine-dithiocarbamate (MGD) and Fe^{2+} (27, 28). We injected MGD and Fe^{2+} into the wild-type and nNOS-null mice at the final stage of 2-week suspension, sacrificed the mice 30 minutes after the injection, and immediately measured the NO levels in muscle tissues. In EPR, the signal height, which is proportional to the amount of NO, was obtained by measuring the peak-to-peak height of the lower field side signal (arrow in Figure 3A) in the characteristic 3-line NO spectrum (29). NO levels in skeletal muscles increased during tail suspension, and the increase was inhibited by daily administration of 7NI to the mice. We used 50 mg/kg of 7NI to selectively inhibit nNOS (30, 31). The increase of NO levels in skeletal muscle during tail suspension was also inhibited by daily administration of 10 mg/kg of N-nitro-L-arginine methylester (L-NAME; pan-NOS inhibitor) (30) to the same extent (data not shown). NO levels in the skeletal muscle of nNOS-null mice after tail suspension were not different from those of ground control mice (Figure 3B), indicating that nNOS is mainly responsible for elevated levels of NO in muscle during tail suspension. Assay of the catalytic activity of NOS showed a higher level in the soluble (cytoplasmic) fraction than in the particulate fraction of suspended wild-type mice (Figure 3C).

Production of NO by nNOS is upstream of Foxo3a pathway. Foxo transcription factors are reported to upregulate many atrophy-related genes and promote muscle atrophy (9, 10). We found that Foxo3a was dephosphorylated and accumulated in the myonuclei of wild-type mice but not nNOS-null mice in western blotting (Figure 4, A and B) and in immunohistochemistry (Supplemental Figure 3). Foxo1 and Foxo4 were not changed during tail suspension in both wild-type and nNOS-null mice (Figure 4B). Recently, several groups have pointed out that the ubiquitin proteasome pathway is largely involved in selective protein degradation during the muscle atrophy process (3, 4). Consistent with this, mRNA levels of 2 muscle-specific E3 ubiquitin ligases, MuRF-1 and atrogin-1/MAFbx, increased during tail suspension in wild-type mice (Figure 4C) (9, 10). Remarkably, the upregulation of these E3 ligases was modest in nNOS-null mice. These observations suggest that nNOS regulates Foxo3a via NO production and thereby upregulates MuRF-1 and atrogin-1/MAFbx. To further examine whether nNOS regulates Foxo3a, we overexpressed nNOS in myotubes by a retrovirus vector (Supplemental Figure 4). Overexpressed nNOS increased both total and nuclear Foxo3a protein levels and decreased phosphorylated Foxo3a in myotubes (Supplemental Figure 4).

NF-κB pathway is activated during muscle atrophy in nNOS-null mice. NF-κB has been shown to be a major regulator of tail suspension–induced

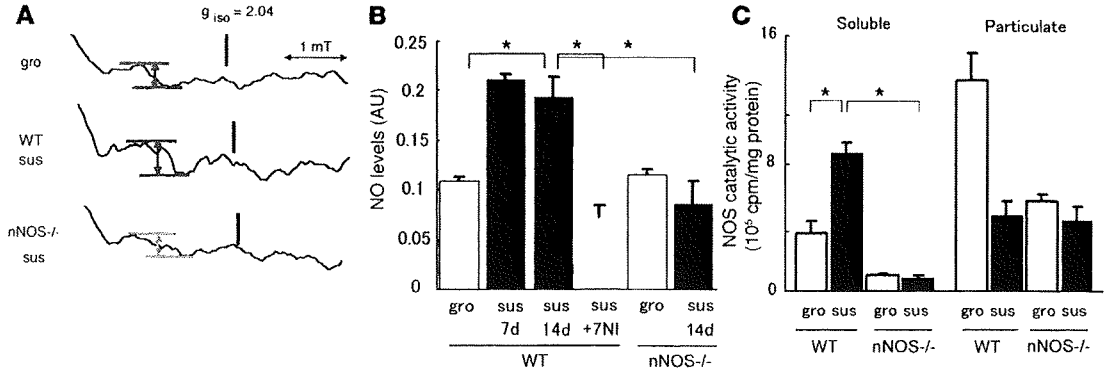

Figure 3

Measurement of NO in muscle and NOS activity during tail suspension. (**A**) EPR spectra of the NO adduct of Fe-MGD complex observed in skeletal muscle at room temperature. The NO-trapping agent was injected 30 minutes before measurements were taken. The EPR spectra of ground control and tail-suspended wild-type and nNOS-null mice were shown. Each spectrum represents the average of 5 accumulations. The signal height was obtained by measuring the peak-to-peak height of the lower field side signal (vertical arrows) in the 3-line spectrum. (**B**) NO levels of the skeletal muscle with and without tail suspension for 7 or 14 days were analyzed in EPR spectrometry ($n = 6$; $^*P < 0.05$, Mann-Whitney). Note that NO level in muscle is elevated in wild-type tail-suspended mice at 14 days but not in nNOS-null tail-suspended mice. 7NI was used as a selective nNOS inhibitor. (**C**) NOS catalytic activity in soluble and particulate fractions ($n = 5$; Mann-Whitney). [^{3}H]-citrulline, converted from [^{3}H]-arginine in vitro by NOS, was quantified by liquid scintillation spectroscopy. Note higher NOS activities in the soluble fraction than in the particulate fraction for suspended wild-type mice.

muscle atrophy (20, 21). EMSA showed that binding activity of NF-κB to its authentic binding sequence is increased by tail suspension in both wild-type and nNOS-null mice (Figure 4D). Importantly, there was no difference between tail-suspended wild-type and nNOS-null mice in the NF-κB binding activity (Figure 4D). In addition, western blotting revealed that p50 is increased by tail suspension (data not shown). These results suggest that NF-κB pathway was activated during tail suspension in the absence of nNOS. Whether the NF-κB activities mediate the residual muscle atrophy that occurred in nNOS-null mice during tail suspension remains to be clarified in a future study.

Inhibitor of NF-κB kinase β is nitrosylated during tail-suspension. Foxo3a is known to be phosphorylated by Akt in skeletal muscle (10, 18). In contrast to our expectation, there was no difference between wild-type and nNOS-null mice in the phosphorylation levels of Akt (Figure 5, A and B). There was no difference between the levels of S6k1 and mammalian target of rapamycin (mTOR), which are under regulation by PI3K/Akt signaling and positively regulate protein synthesis between wild-type and nNOS-null mice during tail suspension (5) (Figure 5A). A recent study reported that NO S-nitrosylates inhibitor of NF-κB kinase β (IKKβ) and thereby inhibits its activity (32). Other reports described inhibition of Foxo3a by IKKβ (33). Intriguingly, we found that tyrosine residues of IKKβ were nitrosylated during tail suspension in wild-type mice but not in nNOS-null mice (Figure 5C). However, whether S-nitrosylation of IKKβ detected during tail suspension contributes to activation of Foxo3a remains to be determined.

7NI alleviates tail suspension–induced muscle atrophy. To further examine the effect of inhibition of nNOS activity on muscle atrophy, 7NI, a nNOS-selective inhibitor, was injected daily into the peritoneal space of the wild-type mice during the 2-week tail suspension (Figure 6). This treatment significantly prevented muscle atrophy during tail suspension but did not increase muscle mass of ground control mice (Figure 6A). 7NI considerably increased phosphorylated Foxo3a and inhibited the increase in dephosphorylated and nuclear Foxo3a during tail suspension (Figure 6C). We also found that upregulation in mRNA levels of MuRF-1 and atrogin-1/MAFbx was abolished by 7NI during tail suspension (Figure 6B). These data imply that nNOS-specific inhibitor is a potential therapeutic strategy for disuse-induced muscle atrophy.

nNOS-null mice show milder muscle atrophy than wild-type mice after cutting of the sciatic nerve. We next examined the role of nNOS in denervation-induced muscle atrophy. Cutting the sciatic nerve on the denervated side resulted in greatly reduced muscle weight 14 days after operation (Figure 7A). Importantly, nNOS had already disappeared from the sarcolemma 3 days after denervation (Figure 7A). We observed much milder muscle atrophy in denervated muscle of nNOS-null mice than wild-type mice (Figure 7B), suggesting that nNOS is also involved in denervation-induced muscle atrophy. We then tested whether an nNOS inhibitor (7NI) or a pan-NOS inhibitor (L-NAME) counteracts denervation-induced muscle atrophy (Figure 7B). These 2 inhibitors limited the muscle atrophy (Figure 7B), indicating that NO is indeed a mediator and therefore a therapeutic target for denervation-induced muscle atrophy.

Discussion

Dislocation of nNOS is a major step in tail suspension–induced muscle atrophy. Involvement of the DGC in cachexia-induced muscle atrophy was recently reported (22). In our report, we demonstrate for what we believe to be the first time that nNOS is dislocated from the sarcolemma to the cytoplasm during tail suspension, whereas other members of the DGC are normally expressed at the sarcolemma. This observation implies that different mechanisms are involved in unloading-induced muscle atrophy and muscle atrophy seen in cachexia. Sarcolemmal nNOS is reported to be a versatile molecule that modulates satellite cell activation (34), formation of neuromuscular junction (35), glucose uptake (36), muscle contraction, and vasodilation (37). To clarify the mechanisms of nNOS translocation, we examined the effects of clenbuterol, streptomycin, and nifedipine on nNOS dislocation during tail suspension. After administration of these drugs, however, we still observed dislocation of nNOS during tail suspension (data not shown). These results suggest that sympathetic nerves, stretch-activated chan-

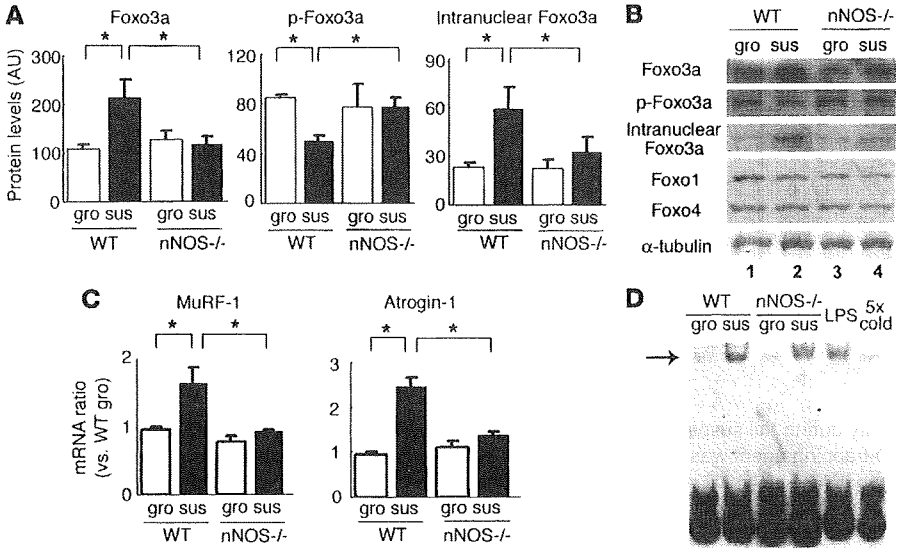

Figure 4

Participation of nNOS in regulation of Foxo3a and upregulation of MuRF-1 and atrogin-1/MAFbx. (**A**) The amounts of total Foxo3a, phosphorylated Foxo3a (p-Foxo3a), and intranuclear Foxo3a in wild-type and nNOS-null muscle during tail suspension were quantified (n = 5). Note that Foxo3a was dephosphorylated and accumulated in the myonuclei of wild-type mice but not of nNOS-null mice. *P < 0.05, Mann-Whitney. (**B**) Representative immunoblot analysis for Foxo3a, phosphorylated Foxo3a, Foxo1, and Foxo4 in total muscle extract, and Foxo3a in nuclear extracts in wild-type ground control (lane 1), wild-type tail-suspended (lane 2), nNOS-null ground control (lane 3), and nNOS-null tail-suspended (lane 4) muscles. α-Tubulin was used as a loading control. (**C**) mRNA levels of ubiquitin ligases (MuRF-1 and atrogin-1/MAFbx) (n = 5) were quantified by real-time RT-PCR. *P < 0.05, Mann-Whitney. (**D**) EMSA of NF-κB. Biotin-labeled double-stranded oligonucleotides containing NF-κB binding sites were incubated with nuclear extracts prepared from ground control and suspended muscles. An arrow indicates the DNA-protein complex. LPS was injected intraperitoneally into mice, and the muscle was used as a positive control for NF-κB binding activity. 5x cold, 5-fold excess of nonlabeled competitors.

nels, and L-type calcium channels are not involved in the dissociation of nNOS from the DGC.

nNOS is anchored at the sarcolemma by interaction with α1-syntrophin (25), a member of the DGC; interestingly, however, α1-syntrophin remains at the sarcolemma during tail suspension (data not shown). To examine whether modification of α1-syntrophin is involved in the dissociation of nNOS from α1-syntrophin, we performed 2-dimensional PAGE and western blotting with anti-α1-syntrophin antibody as previously described (38). The first dimensional isoelectric focusing reveals posttranslational modifications of α1-syntrophin. The results showed slight changes in mobility pattern of α1-syntrophin during tail suspension (data not shown), suggesting that some posttranslational modifications of α1-syntrophin may cause dissociation of nNOS from α1-syntrophin.

Dislocated nNOS leads to production of NO and regulates Foxo/E3 ubiquitin ligases pathway. EPR spectrometry confirmed that cytoplasmic nNOS led to production of NO during tail suspension (Figure 3, A and B). Tail suspension–induced muscle atrophy was blunted in nNOS-null mice (Figure 2, A and B) and 7NI-treated mice (Figure 6A) but not in eNOS-null mice (Figure 2, A and B). iNOS protein was not detected by western blotting in skeletal muscle during tail suspension (data not shown). These data indicate that dislocated nNOS, but neither eNOS nor iNOS, is involved in tail suspension–induced muscle atrophy.

We clearly show that 2 atrophy-related E3 ubiquitin ligases, MuRF-1 and atrogin-1/MAFbx, are not upregulated in nNOS-null muscle during tail suspension (Figure 4C and Figure 6B). Therefore, the induction of these genes is a downstream event of dislocation of nNOS in tail suspension–induced muscle atrophy.

Foxo transcription factors are reported to induce skeletal muscle atrophy by upregulating MuRF-1 or atrogin-1/MAFbx (4, 10, 16, 17). For example, transgenic mice overexpressing Foxo1 in skeletal muscle display a decrease in size of muscle fibers (17). Importantly, Foxo3a remained phosphorylated in nNOS-null mice during tail suspension, and total Foxo3a protein was not increased in tail-suspended nNOS null mice. Moreover, Foxo3a accumulated in the myonuclei of wild-type but not in nNOS-null mice during tail suspension (Figure 4B and Figure 6C).

When we overexpressed nNOS in muscle cells using a retrovirus vector, we found that Foxo3a was activated in nNOS-overexpressing myotubes (Supplemental Figure 4).

How does nNOS/NO regulate Foxo3a pathways? Our observations suggest that nNOS/NO is an upstream regulator of Foxo3a in the tail suspension–induced muscle atrophy process. There are at least 2 possible explanations for how Foxo3a regulates nNOS/NO. First, NO produced by nNOS might inhibit protein kinases, which phosphorylate Foxo3a, thereby protecting Foxo3a from degradation and promoting its translocation from the cytoplasm to the nucleus. There are several kinases that can phosphorylate Foxo, including Akt (10), IKKβ (33), BCR (39), and CDK2 (40). In the present study, we show that Akt activities in nNOS-null muscle were not different from those in wild-type muscle during tail suspension. A fraction of IKKβ was nitrosylated (inactivated) during tail suspension (Figure 5C), but NF-κB was activated in both wild-type and nNOS-null muscle during suspension. This observation suggests that IKKβ activity was not meaningfully disrupted (Figure 4D). Involvement of other kinases remains to be investigated in a future study.

Second, nNOS/NO signal might decrease nuclear export of Foxo3a, resulting in accumulation of Foxo3a in myonuclei and protecting it from phosphorylation by Akt. Foxo is exported from the nucleus in a 14-3-3 protein–dependent process (19), and these molecular interactions remain to be examined.

Dislocation of nNOS and production of NO have no obvious effects on the activity of NF-κB. It has been reported that reduced muscle activity induces muscle atrophy via activation of both Foxo and NF-κB transcription factors (9), at the same time suppressing the Akt pathway (5, 6), resulting in activation of the transcription of MuRF-1 and atrogin-1/MAFbx genes. In this report we demonstrated that dephosphorylation and nuclear accumulation of Foxo3a were largely attenuated in nNOS-null muscle during tail suspension. In contrast, our EMSA assay suggested that the NF-κB pathway was activated in nNOS-null

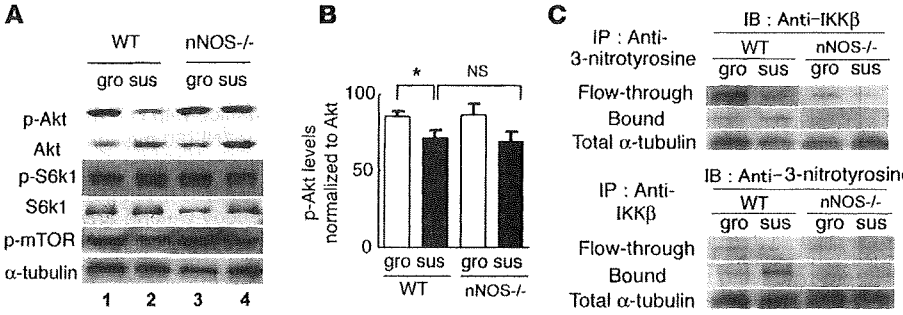

Figure 5

Phosphorylation of Akt and nitrosylation of IKKβ during 2-week tail suspension. (**A**) Immunoblots for protein synthesis pathway components (p-Akt, Akt, p-S6k1, S6k1, and p-mTOR) in wild-type ground control (lane 1), wild-type tail-suspended (lane 2), nNOS-null ground control (lane 3), and nNOS-null tail-suspended (lane 4) muscles. Densities of the bands were normalized to α-tubulin. (**B**) The ratio of phosphorylated Akt to total Akt is shown ($n = 5$; $^*P < 0.05$, Mann-Whitney). (**C**) Detection of nitrosylated IKKβ. Muscle proteins were immunoprecipitated with anti–3-nitrotyrosine antibody (upper panel) or with anti-IKKβ antibody (lower panel) and immunoblotted with anti-IKKβ or anti–3-nitrotyrosine antibodies, respectively. α-Tubulin signals in flow-through fractions are also shown.

mice to a similar extent as in wild-type mice in tail suspension experiments. This observation raises the possibility that NF-κB mediated the residual atrophy that occurred in nNOS-null mice, but further investigation is needed to correctly answer this question.

nNOS and other muscle atrophies. Many conditions induce muscle atrophy, including space flight, immobilization, denervation, cancer cachexia, motor neuron diseases, starvation, and aging (41). Recently it has been reported that muscles of tumor-bearing mice exhibited membrane abnormalities accompanied by reduced levels of dystrophin and increased glycosylation on DGC proteins (22, 23). It was also shown that the DGC could counteract atrophic signaling in cancer cachexia when overexpressed at the sarcolemma (22). In the tail suspension model, we observed dislocation of nNOS but no changes in the sarcolemmal expression of other members of the DGC (Figure 2C). Therefore it is possible that dystrophin deficiency in cancer cachexia induces nNOS dislocation, which results in activation of nNOS and its downstream effectors.

We also found nNOS dislocation in denervation-induced muscle atrophy (Figure 7A). Remarkably, denervation-induced muscle atrophy was modestly blunted in nNOS-null mice or selective nNOS inhibitor–treated mice (Figure 7B). Although iNOS was induced during denervation (data not shown), both 7NI and L-NAME showed a similar effect on muscle atrophy, suggesting that iNOS does not contribute to denervation-induced muscle atrophy.

In conclusion, we demonstrate that nNOS dislocated from the sarcolemma to the cytoplasm in 2 models of disuse-induced muscle atrophy, tail suspension and denervation. We also show that dislocated nNOS led to the production of NO and regulated Foxo3a, MuRF-1, and atrogin-1/MAFbx, key molecules in muscle atrophy. Our model is illustrated in Figure 8. The identification of nNOS as a regulator of unloading-induced muscle wasting suggests that pharmacological intervention targeting nNOS or its downstream or upstream pathways would prevent or diminish this debilitating process.

Methods

Animals and tail suspension model. Twelve-week-old female C57BL/6, nNOS-null and eNOS-null mice were purchased from the Jackson Laboratory. α1-Syntrophin-null mice were produced in our previous study (25). These mice were backcrossed to the C57BL/6 strain for more than 10 generations. The animals were allowed ad libitum access to food and drinking water. The Experimental Animal Care and Use Committee of the National Institute of Neuroscience approved all experimental protocols. The mice were randomly assigned to control or tail suspension groups. To induce muscle atrophy by disuse, mice were suspended so that their hind limbs were 1 mm off the cage floor for 14 days. After 14 days of tail suspension, some groups were allowed 7 days of reloading by normal weight bearing. Muscle weight was normalized to body weight and is presented as a percentage of control in each experiment.

Denervation model. The left sciatic nerve of mice was excised for nearly the full length of the thigh (approximately 10 mm) from a small incision (approximately 4 mm) made in the mid-lateral thigh under general anesthesia under a surgical microscope (Olympus) (42). The mice were sacrificed 3 or 14 days after denervation by cervical dislocation under general anesthesia, and soleus and gastrocnemius muscles were excised for analysis. The right gastrocnemius muscle served as a control.

Reagents. Lipopolysaccharide from *E. coli* (0.1 ml, 3 mg/kg; *E. coli*, serotype 055:B5; Sigma-Aldrich) was administered via intraperitoneal injection. 7NI (Dojindo) was dissolved in peanut oil (50 mg/kg). L-NAME was injected daily into the intraperitoneal cavity of mice (10 mg/kg body weight). Clenbuterol (1 mg/kg; Sigma-Aldrich), streptomycin (300 mg/kg; Sigma-Aldrich) and nifedipine (5 mg/kg; Wako) were dissolved in PBS. PBS was injected into control mice.

Tissue preparation. Control and tail-suspended mice were sacrificed with cervical dislocation. Body and wet muscle were weighed. The gastrocnemius and soleus muscles were collected individually using standard dissection methods and cleaned of excess fat, connective tissue, and tendons. Several of the muscles were frozen in isopentane cooled by liquid nitrogen for histological and immunohistochemical analysis, and the other muscles were frozen directly in liquid nitrogen for RNA isolation or protein extraction and stored at -80°C.

Real time PCR. Total RNA was isolated using TRIzol (GIBCO). For RT-PCR, first-strand cDNA was synthesized using oligo-dT primers. Expression levels of selected genes (nNOS, MuRF-1, atrogin-1/MAFbx, and 18S-rRNA) were analyzed using Applied Biosystems SYBR Green gene expression assays on ABI7700 Sequence Detection System (Applied Biosystems) following the manufacturer's instructions.

H&E staining. Ten-micrometer cryosections were cut in the middle part of the muscle belly to obtain the largest myofiber diameter, placed on poly-L-lysine–coated slides, air dried, and stained with H&E. The sections were viewed and photographed using an HC-2500 digital camera system (Fuji Photo Film).

Immunohistochemistry. Cryostat sections of muscle tissue (10 μm thick), were postfixed in acetone or 4% paraformaldehyde at -20°C and preincubated in PBS containing 5% goat serum and 1% bovine serum albumin for 30 minutes at room temperature. Polyclonal anti-nNOS (Zymed), anti-Foxo3a (Sigma-Aldrich), and anti-laminin-α2 (Alexis) were applied overnight at 4°C. Following incubations with appropriate secondary antibodies, mounted sections were observed by using a Leica confocal microscope. Muscle fiber diameters were determined on cross sections of soleus muscle using the greatest distance between the oppo-

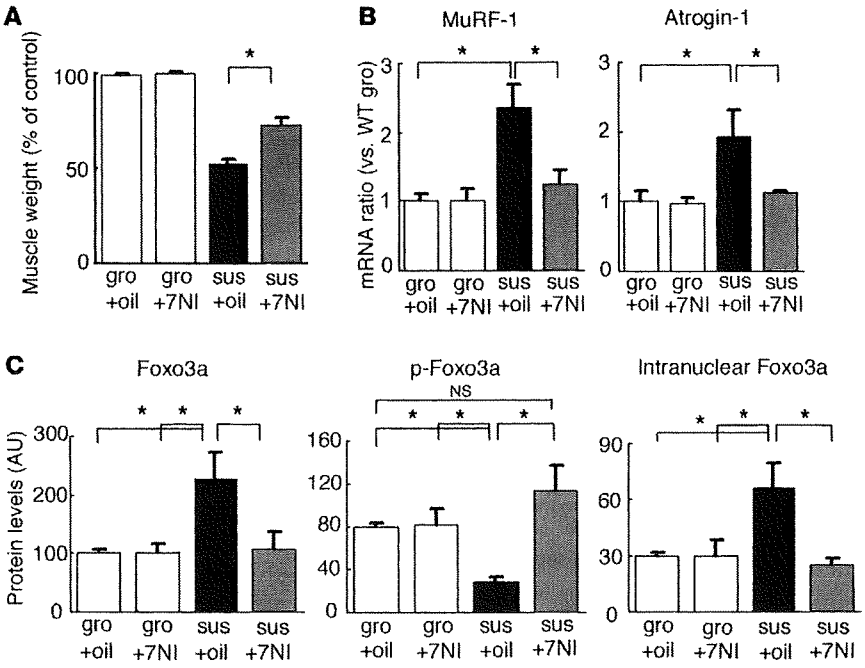

Figure 6
7NI alleviates muscle atrophy during tail suspension. (**A**) Soleus muscle weight of wild-type ground control and wild-type tail-suspended mice with (+7NI) or without 7NI (+oil). Oil or 7NI (50 mg/kg/d) was injected daily into the abdominal cavity of the mice during 2-week tail suspension. Values (muscle weight/body weight) are expressed as percent of wild-type oil-injected muscles after 14-day tail suspension (n = 5–10 per group; $^*P < 0.05$, Mann-Whitney). (**B**) mRNA levels of MuRF-1 and atrogin-1/MAFbx (n = 4) in muscle from wild-type ground control and wild-type tail-suspended mice with or without 7NI were quantified by real-time RT-PCR ($^*P < 0.05$, Mann-Whitney). (**C**) The amount of total Foxo3a, dephosphorylated Foxo3a, and intranuclear Foxo3a (n = 4) were analyzed by western blotting, and band densities were normalized to α-tubulin ($^*P < 0.05$, Mann-Whitney).

site sides of the narrowest aspect of the fiber. Total number of muscle fibers was also counted on cross sections.

Western blotting. Total skeletal muscle protein was extracted from mouse hindlimb muscle for western blot analysis. We used the Bradford method and Coomassie Brilliant Blue G-250 (Bio-Rad) to determine the protein concentrations. Then protein fractions were extracted with a reducing sample buffer containing 10% SDS, 70 mM Tris-HCl, 5% β-mercaptoethanol, and Complete inhibitor cocktail (Roche). Protein (15 or 30 μg per lane) was separated on an SDS-polyacrylamide gel. The resulting gel was subsequently transferred to a polyvinylidene difluoride membrane (Millipore) using 242 mA for 1 hour. The blot was later incubated with primary antibodies. The signals were detected using the enhanced chemiluminescence method (GE Amersham). Relative quantities of proteins in western blots were determined by scanning densitometry (Alpha Innotec) and expressed in arbitrary units. The following antibodies were used for immunoblotting: anti–α1-syntrophin (Biogenesis), anti–laminin-α2 (Alexis), anti-dystrophin (dys2), anti-utrophin, anti–β-dystroglycan, anti-dystrobrevin, anti-dysferlin, anti–caveolin-3 (Novocastra), anti-hsp90 (Stressgen), anti-nNOS, anti-IKKβ, anti-Akt, anti–p-Akt, anti–p-mTOR, anti-p50 (Transduction Laboratories), anti-Foxo3a, anti–p-Foxo3a, anti-Foxo1/4, anti-Na/K-ATPase (Upstate Biotechnology), anti-Hsp70, and anti-iNOS antibody (Santa Cruz Biotechnology Inc.). Anti–α-sarcoglycan antibody was kindly provided by Michihiro Imamura (National Institute of Neuroscience, National Center of Neurology and Psychiatry).

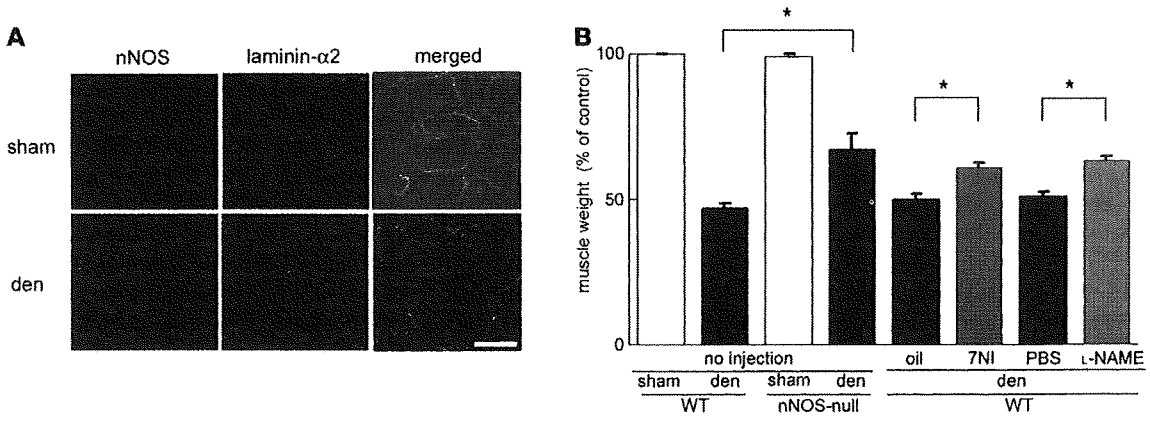

Figure 7
Inhibition of nNOS activities counteracts denervation-induced muscle atrophy. (**A**) Sarcolemmal expression of nNOS in control and denervated muscles. Transverse muscle sections from denervated (den) and sham-operated mice were stained with anti-nNOS (green) and anti–laminin-α2 chain (red) antibodies 3 days after sciatic nerve excision. Scale bar: 50 μm. (**B**) Reduction in soleus muscle weight of wild-type and nNOS-null mice 2 weeks after sham operation or denervation. Weight of wild-type denervated muscle was also measured after 2-week administration of oil, 7NI, PBS, or L-NAME. Values (muscle weight/body weight) were expressed as percentage of the values of sham-operated wild-type muscles (n = 5–10 per group). $^*P < 0.05$, Mann-Whitney.

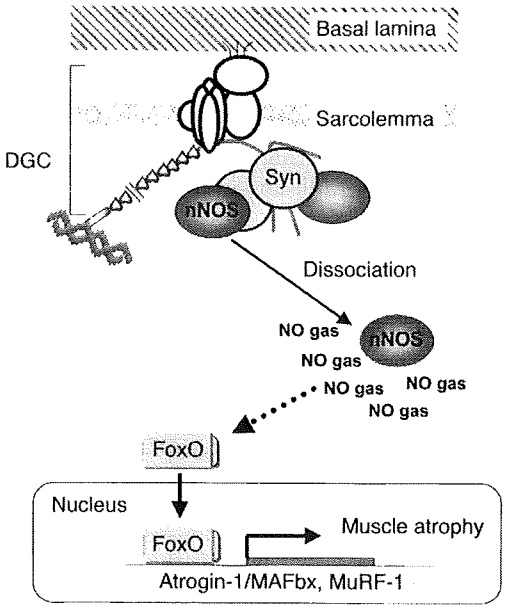

Figure 8
A model of nNOS involvement in tail suspension–induced muscle atrophy. Under normal conditions nNOS is located at the sarcolemma as a peripheral member of the DGC. During tail suspension, nNOS dissociates from α1-sytrophin (syn) and dislocates into the cytoplasm, generating NO, which ultimately regulates Foxo transcription factors, and muscle-specific E3 ubiquitin ligases, MuRF-1, and atrogin-1/MAFbx, which promote muscle protein degradation by the ubiquitin-proteasome system.

Nuclear and cytosolic protein extraction. Nuclear extracts were prepared from mouse skeletal muscle according to the method of Hunter et al. (20). Briefly, the cytosolic extract was obtained from the first supernatant of the nuclear extract preparation. The supernatant was placed in Millipore Ultrafree-4 centrifugal columns that had been pre-wetted with 0.5 ml of dilution buffer (20 mM HEPES, 40 mM KCl, 10% glycerol, 0.2 mM EDTA, 1 mM DTT), and centrifuged (7,500 *g*) at 4°C for 30 minutes. Dilution buffer (0.8 ml) was added to the column, and the 30-minute spin was repeated. Protein concentrations were determined using the Bradford protein assay (Bio-Rad).

Immunoprecipitation. Skeletal muscle samples were homogenized in 0.15 M NaCl, 10 mM HEPES (pH 7.5) and Complete inhibitor cocktail (Roche), with or without 1% digitonin (Wako). nNOS and caveolin-3 immunoprecipitation was performed with anti-nNOS goat polyclonal antibody (Santa Cruz Biotechnology Inc.) and anti-caveolin-3 antibody (Transduction Laboratories). The samples were incubated with protein G gel (GE Amersham) overnight at 4°C. After the gel was washed with the equilibrating buffer, the bound fraction was eluted with 1% SDS, 1 mM tris-(2-carboxyethyl) phosphine, and 14 mM Tris-HCl (pH 6.7) and concentrated. Coimmunoprecipitates were resolved by SDS-PAGE and analyzed by western blotting. α-Tubulin was used as internal control for total protein inputted.

Two-dimensional PAGE. Muscle extracts from ground control and tail suspension mice were resolved on 2-dimensional PAGE and analyzed by western blotting as described in ref. 38.

EMSA. EMSA was performed according to the manufacturer's instructions (Panomics). Briefly, probes were end-labeled with biotin. Binding reactions were performed for 30 minutes in a volume of 10 ml. Specificity of DNA binding was determined by addition of a 5-fold molar excess of unlabeled competitor DNA to the binding reactions. The binding reactions were loaded onto 6% non-denaturing polyacrylamide gels and electrophoretically resolved in 0.5× tris-borate EDTA (TBE) buffer.

NOS catalytic assays. NOS catalytic assays were carried out according to the method described by Brenman et al. (24). Muscles from wild-type and nNOS-null mice with or without tail suspension were homogenized in 10 volumes of buffer containing 25 mM Tris-HCl, pH 7.4, 1 mM EDTA, 1 mM EGTA, and 0.1 mM NaCl. The homogenate was centrifuged at 20,000 *g* to separate the soluble fraction. The pellet was extracted in the same buffer containing 0.5 M NaCl and centrifuged at 20,000 *g* to create a particulate fraction. Aliquots from these fractions were assayed in 125-μl reactions containing 1.8×10^5 cpm of [^{3}H]-arginine (53.0 Ci/mmol; GE Amersham), 1 mM NADPH, 640 μM $CaCl_2$, 1 μM calmodulin, and 3 μM each of tetrahydrobiopterin, FAD, and FMN. After incubation for 20 minutes at 37°C, the assays were terminated with 2 ml of 20 mM HEPES, pH 5.5, and 2 mM EDTA. The samples were then applied to AG50WX-8 columns (Na^+ form; Dowex), which were centrifuged, and the supernatant was collected. [^{3}H]-citrulline was quantified by liquid scintillation spectroscopy.

Subcellular fractionation. The subcellular fractionation was performed according to the method described by Brenman et al. (24). The gastrocnemius muscle was homogenized in 10 volumes (w/v) of buffer A (25 mM Tris-HCl, pH 7.4, 100 mM NaCl, 1 mM EDTA, 1 mM EGTA). The nuclei of the muscle were pelleted by centrifugation at 1,000 *g*. The supernatant was then centrifuged at 20,000 *g* to yield the supernatant S1. The resulting heavy microsomal pellet was resuspended in buffer B (500 mM NaCl added to buffer A), incubated for 30 minutes at 4°C with agitation, and centrifuged at 15,000 *g*, yielding supernatant S2. The pellet from this last centrifugation was resuspended in buffer B containing 0.5% Triton X-100, incubated for 30 minutes at 4°C with agitation, and centrifuged at 15,000 *g* to create supernatant S3 and the final pellet. The fractions were resolved using the sample buffer and analyzed by SDS-polyacrylamide gel electrophoresis. The proteins were transferred to a polyvinylidene difluoride membrane (Millipore), which was later incubated with anti-nNOS antibody. The bands were quantified in densitometry.

Direct measurement of NO by EPR spectrometry. Concentrations of NO in the skeletal muscle of mice were measured using the NO-trapping technique combined with EPR spectroscopy (29). Spin traps react with unstable free radicals such as NO to form a relatively stable radical adduct. This long-lived adduct formation results in accumulation of a steady-state formation of these free radicals, and thus the resultant radical adduct can be detected readily by EPR spectroscopy. We used a Fe-MGD complex as the trapping agent to quantify NO levels in the skeletal muscle tissues of the mice. Solutions of $FeSO_4$ (62 mg/kg; Wako) and MGD (348 mg/kg; Dojindo) were injected subcutaneously. The Fe-MGD complex formed had a high specificity for NO (27, 29), and the NO-Fe-MGD complex was detected by EPR spectroscopy. The amplitude of the signal measured from the peak-to-peak height of the lower field side signal in the 3-line spectrum is known to be proportional to the amount of NO (29). The level of NO-Fe-MGD complex was estimated by comparing it with the signal height of a standard solution of a chemically synthesized NO complex. The concentration in tissues was determined 30 minutes after injection of the NO-trapping reagent. Thirty minutes after administration of the reagent, the gastrocnemius and soleus muscle were removed and weighed (approximately 100–120 mg). The tissue was minced and subjected to immediate measurement of NO by EPR spectrometry. X-band EPR spectra were measured at room temperature with a TE-200 EPR spectrometer (JEOL). The homogenates were drawn into a capillary tube (75 mm in length, 46 μl in internal volume) that had been inserted first into an EPR quartz tube (outside diameter, 5 mm), then introduced into the cavity. The instrument settings were as follows: center field, 331 mT; field scan, 4 mT; sweep time, 2 min; time

constant, 0.3 s; modulation amplitude, 0.32 mT; modulation frequency, 9.44 GHz; microwave power, 60 mW.

Statistics. Statistical differences were determined by either 2-tailed unpaired Student's *t* test or the Mann-Whitney test. All data are expressed as mean ± SEM. Statistical significance is defined as $P < 0.05$.

Acknowledgments

We thank S. Masuda, A. Fukase, and T. Harano for technical support; K. Asanuma and J. Yoshitake for EPR spectrometry; Y. Onodera and M. Tateyama for immunohistochemistry; and all members of the Department of Molecular Therapy, National Institute of Neuroscience, for technical assistance and useful discussion, especially M. Yoshida, M. Ikemoto, and Y. Mochizuki. We also thank K. Ono for correcting our English. This work was supported by Research on Nervous and Mental Disorders (grant 16B-2); Health Science Research Grants for research on the human genome and gene therapy (H16-genome-003) and for research on brain science (H15-kokoro-021 and H18-kokoro-019) from the Japanese Ministry of Health, Labor and Welfare; Grants-in-Aid for Scientific Research (14657158, 15390281, 16590333, 17590857, and 18590392) from the Japanese Ministry of Education, Culture, Sports, Science and Technology; and the Ground-based Research Program for Space Utilization, promoted by Japan Space Forum.

Received for publication October 16, 2006, and accepted in revised form May 29, 2007.

Address correspondence to: Shin'ichi Takeda, Department of Molecular Therapy, National Institute of Neuroscience, National Center of Neurology and Psychiatry, 4-1-1 Ogawa-higashi, Kodaira, Tokyo 187-8502, Japan. Phone: 81-42-346-1720; Fax: 81-42-346-1750; E-mail: takeda@ncnp.go.jp.

1. Tidball, J.G. 2005. Mechanical signal transduction in skeletal muscle growth and adaptation. *J. Appl. Physiol.* **98**:1900–1908.
2. Ikemoto, M., et al. 2001. Space shuttle flight (STS-90) enhances degradation of rat myosin heavy chain in association with activation of ubiquitin-proteasome pathway. *FASEB J.* **15**:1279–1281.
3. Bodine, S.C., et al. 2001. Identification of ubiquitin ligases required for skeletal muscle atrophy. *Science.* **294**:1704–1708.
4. Gomes, M.D., Lecker, S.H., Jagoe, R.T., Navon, A., and Goldberg, A.L. 2001. Atrogin-1, a muscle-specific F-box protein highly expressed during muscle atrophy. *Proc. Natl. Acad. Sci. U. S. A.* **98**:14440–14445.
5. Bodine, S.C., et al. 2001. Akt/mTOR pathway is a crucial regulator of skeletal muscle hypertrophy and can prevent muscle atrophy in vivo. *Nat. Cell Biol.* **3**:1014–1019.
6. Song, Y.H., et al. 2005. Muscle-specific expression of IGF-1 blocks angiotensin II-induced skeletal muscle wasting. *J. Clin. Invest.* **115**:451–458. doi:10.1172/JCI200522324.
7. Rommel, C., et al. 2001. Mediation of IGF-1-induced skeletal myotube hypertrophy by PI(3)K/Akt/mTOR and PI(3)K/Akt/GSK3 pathways. *Nat. Cell Biol.* **3**:1009–1013.
8. Latres, E., et al. 2005. Insulin-like growth factor-1 (IGF-1) inversely regulates atrophy-induced genes via the phosphatidylinositol 3-kinase/Akt/mammalian target of rapamycin (PI3K/Akt/mTOR) pathway. *J. Biol. Chem.* **280**:2737–2744.
9. Cai, D., et al. 2004. IKKbeta/NF-kappaB activation causes severe muscle wasting in mice. *Cell.* **119**:285–298.
10. Sandri, M., et al. 2004. Foxo transcription factors induce the atrophy-related ubiquitin ligase atrogin-1 and cause skeletal muscle atrophy. *Cell.* **117**:399–412.
11. Li, Y.P., Schwartz, R.J., Waddell, I.D., Holloway, B.R., and Reid, M.B. 1998. Skeletal muscle myocytes undergo protein loss and reactive oxygen-mediated NF-kappaB activation in response to tumor necrosis factor alpha. *FASEB J.* **12**:871–880.
12. Greer, E.L., and Brunet, A. 2005. FOXO transcription factors at the interface between longevity and tumor suppression. *Oncogene.* **24**:7410–7425.
13. Lehtinen, M.K., et al. 2006. A conserved MST-FOXO signaling pathway mediates oxidative-stress responses and extends life span. *Cell.* **125**:987–1001.
14. Matsumoto, M., Han, S., Kitamura, T., and Accili, D. 2006. Dual role of transcription factor FoxO1 in controlling hepatic insulin sensitivity and lipid metabolism. *J. Clin. Invest.* **116**:2464–2472. doi:10.1172/JCI27047.
15. Berman, J., and Kenyon, C. 2006. Germ-cell loss extends C. elegans life span through regulation of DAF-16 by kri-1 and lipophilic-hormone signaling. *Cell.* **124**:1055–1068.
16. Lecker, S.H., et al. 2004. Multiple types of skeletal muscle atrophy involve a common program of changes in gene expression. *FASEB J.* **18**:39–51.
17. Kamei, Y., et al. 2004. Skeletal muscle FOXO1 (FKHR) transgenic mice have less skeletal muscle mass, down-regulated Type I (slow twitch/red muscle) fiber genes, and impaired glycemic control. *J. Biol. Chem.* **279**:41114–41123.
18. Skurk, C., et al. 2005. The FOXO3a transcription factor regulates cardiac myocyte size downstream of AKT signaling. *J. Biol. Chem.* **280**:20814–20823.
19. Obsilova, V., et al. 2005. 14-3-3 Protein interacts with nuclear localization sequence of forkhead transcription factor FoxO4. *Biochemistry.* **44**:11608–11617.
20. Hunter, R.B., et al. 2002. Activation of an alternative NF-kappaB pathway in skeletal muscle during disuse atrophy. *FASEB J.* **16**:529–538.
21. Hunter, R.B., and Kandarian, S.C. 2004. Disruption of either the Nfkb1 or the Bcl3 gene inhibits skeletal muscle atrophy. *J. Clin. Invest.* **114**:1504–1511. doi:10.1172/JCI200421696.
22. Acharyya, S., et al. 2005. Dystrophin glycoprotein complex dysfunction: A regulatory link between muscular dystrophy and cancer cachexia. *Cancer Cell.* **8**:421–432.
23. Acharyya, S., et al. 2004. Cancer cachexia is regulated by selective targeting of skeletal muscle gene products. *J. Clin. Invest.* **114**:370–378. doi:10.1172/JCI200420174.
24. Brenman, J.E., Chao, D.S., Xia, H., Aldape, K., and Bredt, D.S. 1995. Nitric oxide synthase complexed with dystrophin and absent from skeletal muscle sarcolemma in Duchenne muscular dystrophy. *Cell.* **82**:743–752.
25. Kameya, S., et al. 1999. Alpha1-syntrophin gene disruption results in the absence of neuronal-type nitric-oxide synthase at the sarcolemma but does not induce muscle degeneration. *J. Biol. Chem.* **274**:2193–2200.
26. Hosaka, Y., et al. 2002. Alpha1-syntrophin-deficient skeletal muscle exhibits hypertrophy and aberrant formation of neuromuscular junctions during regeneration. *J. Cell Biol.* **158**:1097–1107.
27. Lecour, S., et al. 2001. Levels of nitric oxide in the heart after experimental myocardial ischemia. *J. Cardiovasc. Pharmacol.* **37**:55–63.
28. Asanuma, K., et al. 2005. Diffusion of cytotoxic concentrations of nitric oxide generated luminally at the gastro-oesophageal junction of rats. *Gut.* **54**:1072–1077.
29. Nagano, T., and Yoshimura, T. 2002. Bioimaging of Nitric Oxide. *Chem. Rev.* **102**:1235–1270.
30. Kato, N., Sato, S., Yokoyama, H., Kayama, T., and Yoshimura, T. 2005. Sequential changes of nitric oxide levels in the temporal lobes of kainic acid-treated mice following application of nitric oxide synthase inhibitors and phenobarbital. *Epilepsy Res.* **65**:81–91.
31. Moore, P.K., and Bland-Ward, P.A. 1996. 7-nitroindazole: an inhibitor of nitric oxide synthase. *Methods Enzymol.* **268**:393–398.
32. Reynaert, N.L., et al. 2004. Nitric oxide represses inhibitory kappaB kinase through S-nitrosylation. *Proc. Natl. Acad. Sci. U. S. A.* **101**:8945–8950.
33. Hu, M.C., et al. 2004. IkappaB kinase promotes tumorigenesis through inhibition of forkhead FOXO3a. *Cell.* **117**:225–237.
34. Segalat, L., Grisoni, K., Archer, J., Vargas, C., Bertrand, A., and Anderson, J.E. 2005. CAPON expression in skeletal muscle is regulated by position, repair, NOS activity, and dystrophy. *Exp. Cell Res.* **302**:170–179.
35. Shiao, T., et al. 2004. Defects in neuromuscular junction structure in dystrophic muscle are corrected by expression of a NOS transgene in dystrophin-deficient muscles, but not in muscles lacking alpha- and beta1-syntrophins. *Ham. Mol. Genet.* **13**:1873–1884.
36. Kapur, S., Bedard, S., Marcotte, B., Cote, C.H., and Marette, A. 1997. Expression of nitric oxide synthase in skeletal muscle: a novel role for nitric oxide as a modulator of insulin action. *Diabetes.* **46**:1691–1700.
37. Stamler, J.S., and Meissner, G. 2001. Physiology of nitric oxide in skeletal muscle. *Physiol. Rev.* **81**:209–237.
38. Yoshida, M., et al. 1995. Dystrophin-associated protein A0 is a homologue of the Torpedo 87K protein. *FEBS Lett.* **367**:311–314.
39. Yusuf, I., Zhu, X., Kharas, M.G., Chen, J., and Fruman, D.A. 2004. Optimal B-cell proliferation requires phosphoinositide 3-kinase-dependent inactivation of FOXO transcription factors. *Blood.* **104**:784–787.
40. Huang, H., Regan, K.M., Lou, Z., Chen, J., and Tindall, D.J. 2006. CDK2-dependent phosphorylation of FOXO1 as an apoptotic response to DNA damage. *Science.* **314**:294–297.
41. Kandarian, S.C., and Jackman, R.W. 2006. Intracellular signaling during skeletal muscle atrophy. *Muscle Nerve.* **33**:155–165.
42. Mochizuki, Y., et al. 2005. Participation of bone marrow-derived cells in fibrotic changes in denervated skeletal muscle. *Am. J. Pathol.* **166**:1721–1732.

Autologous Transplantation of SM/C-2.6$^+$ Satellite Cells Transduced with Micro-dystrophin *CS1* cDNA by Lentiviral Vector into *mdx* Mice

Madoka Ikemoto[1], So-ichiro Fukada[1], Akiyoshi Uezumi[1], Satoru Masuda[1], Hiroyuki Miyoshi[2], Hiroshi Yamamoto[3], Michiko R Wada[1], Nami Masubuchi[1,4], Yuko Miyagoe-Suzuki[1] and Shin'ichi Takeda[1]

[1]*Department of Molecular Therapy, National Institute of Neuroscience, National Center of Neurology and Psychiatry, Kodaira, Tokyo, Japan;* [2]*BioResource Center, RIKEN Tsukuba Institute, Tsukuba, Ibaraki, Japan;* [3]*Department of Immunology, Graduate School of Pharmaceutical Sciences, Osaka University, Suita, Osaka, Japan;* [4]*Laboratory of Molecular Embryology, Department of Bioscience, Kitasato University School of Science, Sagamihara, Kanagawa, Japan*

Duchenne muscular dystrophy (DMD) is a lethal muscle disorder caused by mutations in the dystrophin gene. Transplantation of autologous myogenic cells genetically corrected *ex vivo* is a possible treatment for this disorder. In order to test the regenerative efficiency of freshly isolated satellite cells, we purified quiescent satellite cells from limb muscles of 8–12-week-old green fluorescent protein-transgenic (GFP-Tg) mice using SM/C-2.6 (a recently developed monoclonal antibody) and flow cytometry. Freshly isolated satellite cells were shown to participate in muscle regeneration more efficiently than satellite cell-derived myoblasts passaged *in vitro* do, when transplanted into tibialis anterior (TA) muscles of 8–12-week-old cardiotoxin-injected C57BL/6 mice and 5-week-old dystrophin-deficient *mdx* mice, and analyzed at 4 weeks after injection. Importantly, expansion of freshly isolated satellite cells *in vitro* without passaging had no detrimental effects on their regenerative capacity. Therefore we directly isolated satellite cells from 5-week-old *mdx* mice using SM/C-2.6 antibody and cultured them with lentiviral vectors expressing micro-dystrophin *CS1*. The transduced cells were injected into TA muscles of 5-week-old *mdx* mice. At 4 weeks after transplantation, the grafted cells efficiently contributed to regeneration of *mdx* dystrophic muscles and expressed micro-dystrophin at the sarcolemma. These results suggest that there is potential for lentiviral vector-mediated *ex vivo* gene therapy for DMD.

Received 22 February 2007; accepted 28 July 2007; published online 28 August 2007. doi:10.1038/sj.mt.6300295

INTRODUCTION

Duchenne muscular dystrophy (DMD) is an X-linked, lethal disorder of skeletal muscle caused by mutations in the dystrophin gene.[1] Dystrophin is a 427 kd large sub-sarcolemmal protein that forms the dystrophin/glycoprotein complex at the sarcolemma with α- and β-dystroglycans, α-, β-, γ-, and δ-sarcoglycans, and other molecules, and links the cytoskeleton with the basal lamina.[2,3] The lack of dystrophin in the sarcolemma causes instability of the muscle membrane, leading to muscle degeneration and myofiber loss. Although there is no effective treatment for the disease at present, cell therapy could be a promising approach. Satellite cells are quiescent mononucleated cells located external to the muscle membrane but internal to the basal lamina in adult skeletal muscle.[4] On muscle damage, they activate, proliferate, and then exit the cell cycle either to differentiate into mature myofibers or to renew the quiescent satellite cell pool. Because satellite cells have robust regenerative capacity,[5,6] they are expected to be a feasible source for cell therapy in DMD. Indeed, transplantation of myoblasts successfully restored dystrophin expression in dystrophin-deficient muscle under immunosuppression.[7,8] Nevertheless, in the early 90s, transplantation of satellite cell-derived myoblasts failed to improve muscle force in DMD patients.[9–11] The failure has been ascribed to poor survival[12–14] and limited distribution of the transplanted cells after injection.[15] The latter problem could possibly be partly overcome by using high-density injections of myoblasts.[16,17] On the other hand, the mechanisms by which grafted myoblasts are rapidly lost after injection have not been fully addressed.[12–14]

Many studies have employed crude cell preparations containing both satellite cells and non-myogenic cells[18,19] or satellite cell-derived myoblasts extensively amplified *in vitro*.[15,20–22] In a recent study, Montarras *et al.* directly isolated (Pax3)green fluorescent protein (GFP)-expressing satellite cells from the diaphragm of adult *Pax3*$^{GFP/+}$ mice by flow cytometry.[23] These cells constituted a homogeneous population and the majority were quiescent. When grafted into irradiated muscles of immunodeficient *nu/nu* dystrophin-deficient *mdx* mice, the freshly isolated satellite cells efficiently contributed to both fiber repair and the muscle satellite cell compartment,[23] thereby suggesting that fresh satellite cells are a potential source for cell therapy in DMD.

For transplanting autologous cells, which are expected to evade the host immune response to grafted cells, the lentiviral vector is a potential tool for introducing the therapeutic gene

Correspondence: Shin'ichi Takeda, Department of Molecular Therapy, National Institute of Neuroscience, National Center of Neurology and Psychiatry, 4-1-1 Ogawa-higashi, Kodaira, Tokyo 187-8502, Japan. E-mail: takeda@ncnp.go.jp